Mineralogical Magazine, February 2007, Vol. 71(1), pp. 17–40

The texture and composition of tourmaline in metasediments of the Sinai, Egypt: Implications for the tectono-metamorphic evolution of the Pan-African basement

M. M. Abu El-Enen[1,*] and M. Okrusch[2]

[1]Department of Geology, Faculty of Science, El Mansoura University, El Mansoura 35516, Egypt
[2] Mineralogisches Institut, Universität Würzburg, Am Hubland, D-97074, Würzburg, Germany

[*Received 14 March 2006; Accepted 8 May 2007*]

ABSTRACT

Accessory tourmaline in metasediments from the Sinai crystalline basement exhibits textural and chemical signatures that relate to the evolution of regional metamorphism and deformation during the Pan-African orogeny and testifies to different *P-T* path segments. Tourmaline inclusions in various porphyroblasts were formed during the prograde phase of metamorphism; acicular to prismatic crystals in the matrix, oriented sub-parallel to, and enveloped by, the main foliation crystallized syntectonically under prograde and peak metamorphic conditions; tourmaline cross-cutting the main foliation may have formed just after the peak or during the retrograde phase of metamorphism. Some of the cores in tourmaline crystals, showing different colours, are interpreted as former detrital grains. The abundance of tourmaline decreases with increasing peak metamorphic conditions. The tourmaline investigated belongs to the schorl–dravite$_{ss}$ group, generally with X_{Mg} of 0.42−0.73 and X_{Ca} = Ca/(Ca+Na+K+□) of 0.02−0.24, typical of tourmalines in metapelites and metapsammites; whereas detrital cores have been derived from various sources, including former tourmaline-quartz and pre-existing high-metamorphic rocks. Tourmaline of the Sinai metasediments was formed during metamorphism of the sedimentary precursors, essentially in a closed system, where clay minerals and organic matter, together with detrital tourmaline, served as the source of boron. Although a metamorphic facies should be defined by characteristic mineral assemblages present in metamorphic rocks, tourmaline chemistry is a good monitor of *P-T* conditions in the metapelites and semi-metapelites investigated, showing an increase in X_{Mg} with increasing metamorphic grade, where X^{tur}_{Mg} = 0.60 distinguishes between greenschist and lower-amphibolite facies, while X^{tur}_{Mg} = 0.65 could distinguish lower- from middle- to upper-amphibolite facies. The results of tourmaline-biotite geothermometry compare well with our former temperature estimates using conventional geothermometry and phase-diagram modelling.

Keywords: tourmaline, Pan-African, Sinai, metasediments, metamorphic grade, tourmaline-biotite geothermometry, boron.

Introduction

Tourmaline is a common accessory mineral in igneous and metamorphic rocks. During metamorphism, it may occur as a product of boron metasomatism from external fluids in an open system, e.g. in contact aureoles (e.g. Dutrow *et al.*, 1999). However, metamorphic tourmaline is formed more commonly in a nearly closed system, either by recrystallization of detrital tourmaline grains or by prograde reactions, involving boron adsorbed at the clay fraction of the pre-existing sediments, or both. Tourmaline in metamorphic rocks has a wide stability range from greenschist to amphibolite facies (Henry and

* E-mail: mahrous@mans.edu.eg
DOI: 10.1180/minmag.2007.071.1.17

Guidotti, 1985; Henry and Dutrow, 1996; Michailidis *et al*; 1996), but breaks down at higher temperatures corresponding to the upper amphibolite and granulite facies (Henry and Dutrow, 1996; Kawakami, 2001; Kawakami and Ikeda, 2003). Variability of tourmaline composition may reflect physical and chemical changes during crystallization of the host rocks, and thus has a potential for preserving chemical signatures through multiple metamorphic (or hydrothermal) events (Slack and Coad, 1989; Bröcker and Franz, 2000). Therefore, tourmaline can be used to monitor metamorphic conditions, e.g. by its increase in X_{Mg} = Mg/(Mg+Fe^{tot}) with metamorphic grade (Henry and Dutrow, 1996; Colopietro and Friberg, 1987; Henry, 2003). Distinct optical and compositional zoning in tourmaline is recorded up to the lower sillimanite zone, but becomes more and more blurred in higher-grade rocks due to intensified diffusion (Henry and Dutrow, 1996; Sperlich *et al.*, 1996). Furthermore, tourmaline chemistry has been employed as a petrogenetic provenance indicator in clastic sedimentary and metasedimentary rocks (Henry and Guidotti, 1985; Henry and Dutrow, 1992). Tourmaline from metapelites belongs essentially to the schorl−dravite solid solution, with smaller amounts of the uvite/feruvite and foitite/Mg-foitite components (e.g. Henry and Dutrow, 1996).

In the Egyptian basement, tourmaline of the schorl–dravite variety was reported from Wadi Sikait, central Eastern Desert (Hashad, 2001; Harraz and El-Sharkawy, 2001), where it was

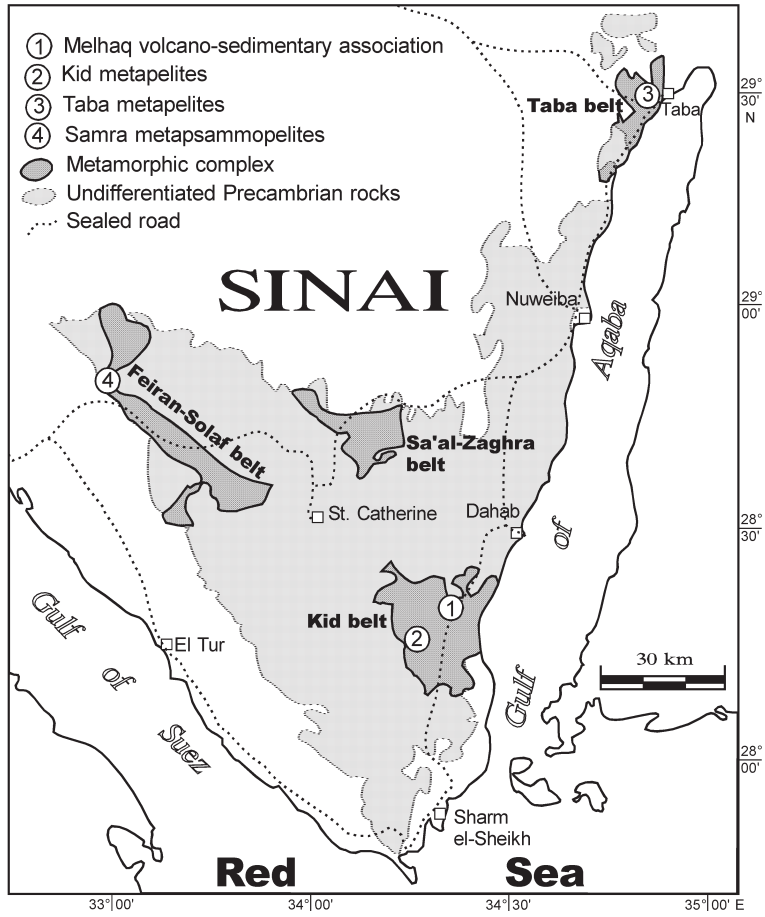

FIG. 1. Sketch map of southern Sinai showing the Precambrian basement exposure and its four metamorphic complexes.

formed presumably as a result of metasomatic exchange of boron-rich magmatic-hydrothermal fluids with Mg-rich host rocks (Harraz and El-Sharkawy, 2001). So far, detailed studies concerned with metamorphic tourmalines in the Egyptian basement have not been carried out. The aim of the present study is to characterize tourmaline in metasediments from different parts of the crystalline basement in the Sinai Peninsula. Textural and compositional evidence will be used to manifest different stages of tourmaline growth in the course of the tectono-metamorphic evolution of the hosting metasediments. Metamorphic temperatures were estimated by the empirically calibrated tourmaline-biotite geothermometer of Colopietro and Friberg (1987) and compared with our previous results from conventional geothermobarometry and phase diagram modelling (Abu El-Enen *et al.*, 2003, 2004).

Geological setting, rock types and mineral assemblages

The crystalline basement, exposed in the southern part of the Sinai Peninsula, belongs to the northernmost region of the Arabian-Nubian Shield, which represents a juvenile, arc-accreted terrane, formed in Neoproterozoic times by the collision of East and West Gondwana and closure of the Mozambique Ocean (e.g. Shackleton, 1986, 1996; Kröner *et al.*, 1987; Dixon and Golombek, 1988; Rogers *et al.*, 1995; Teklay *et al.*, 1998; Stern, 1994, 2002). Metamorphic rocks cover about one-third of the basement exposure. They comprise strongly deformed and metamorphosed sediments, arc volcanites and calc-alkaline granitoids, which underwent a single metamorphic event at low-pressure, greenschist to amphibolite-facies conditions (e.g. Shimron and Zwart, 1970; Reymer *et al.*, 1984; Abu El-Enen, 1995; Cosca *et al.*, 1999; Abu El-Enen *et al.*, 2003, 2004; Brooijmans *et al.*, 2003). The metamorphic rocks were intruded by voluminous late- to post-orogenic granitoid plutons and separated into four metamorphic complexes, namely the Taba complex in the northeast, the Kid complex in the southeast, the Sa'al-Zaghra complex in the centre, and the Feiran-Solaf complex in the west of the exposed basement (Fig. 1). Tourmaline was investigated in metamorphosed pelites, psammopelites and calcpelites of the Kid, Taba and Feiran-Solaf metamorphic complexes. The mineral contents of the samples investigated are listed in Table 1.

The Kid complex consists of a volcano-sedimentary succession with island-arc geochemical affinity. Metamorphism increases towards the central and northern parts of the complex (Shimron, 1980; Navon and Reymer, 1984; Abu El-Enen *et al.*, 2003; Abu El-Enen and Makroum, 2003; Brooijmans *et al.*, 2003). In the Wadi Kid–Wadi Umm Zariq area, the western central part of the Kid complex, the following near-peak metamorphic assemblage in metapelites of the Umm Zariq Formation have been recorded: Qtz + Pl (An_{20-38}) + Ms + Bt + Grt + And ± St ± Crd ± Sil + Tur + Ilm, which conforms to lower-amphibolite facies at relatively low pressures, i.e. 540–590ºC, 3–4 kbar (Reymer *et al.*, 1984; Abu El-Enen *et al.*, 2003).

A larger area, extending from the entrance of Wadi Madsus in the south to the northernmost border of the Kid complex is occupied by the volcano-sedimentary association of the Melhaq Formation. It consists of metapelites and volcanogenic metagreywackes, interbedded and intercalated with acidic to predominantly basic metavolcanites. The metamorphic grade of this association increases northward. In the south, metacalcpelites contain the upper-greenschist facies assemblage Qtz + Ab + Ep + Ms + Chl + Bt + Tur + Mag. In the central part, near-peak assemblages Qtz + Pl (An_{19-26}) + Bt ± Ms ± Grt ± Kfs + Tur + Mag, testifying to the lower-amphibolite facies, predominate in pelitic beds and in the matrix between clasts in the greywacke samples (Shimron, 1984; Furnes *et al.*, 1985; authors' unpublished observations). In the extreme northern and northeastern parts of the Melhaq Formation, coarse-grained metapelitic schists display the near-peak assemblages Qtz-Pl (An_{28-39}) + Bt + Grt ± Crd ± Sil (fibrolite) ± Ep ± Kfs ± Ilm ± Mag + Tur conforming to the upper-amphibolite facies with *P-T* conditions at 640–700ºC and 4.3–4.6 kbar (Abu El-Enen and Makroum, 2003; and authors' unpublished observations).

The Taba complex, in the extreme northeastern part of the exposed Sinai basement (Fig. 1), is composed of metapelites, metagabbros-metadiorites, orthogneisses and migmatites (Eyal, 1980; Abu El-Enen, 1995; Abu El-Enen *et al.*, 1999, 2004). In the northern part of the Taba complex, near-peak mineral assemblages in metapelites are Qtz-Pl (An_{22-37}) + Bt + Grt ± St ± pinitized Crd ± And ± Sil ± Rt ± Mag ± Ilm ± Tur. They were formed under amphibolite-facies conditions with peak temperatures at 550–590ºC and pressures of 3–5 kbar (Abu El-Enen *et al.*, 2004).

TABLE 1. Mineral contents in the samples investigated (Mineral abbreviations after Kretz, 1983).

Area	Melhaq							W. Kid–W. Umm Zariq						Taba				G. Samra	
	Southern		Central			Northern													
S. no.	M28	M34	M38	M43	M46	M47	M50	K6	K9	K14	K22	K25	K35	T2	T3	T10	T12	Z1	Z3
Qtz	◇	◇	◇	◇	◇	◇	◇	◇	◆	◇	◇	◇	◇	◆	◆	◆	◆	◇	◇
Pl	*	*	◇	◇	*	*	*	*	*	*	*	*	*	*	*	*	*	◆	◆
Kf	–	–	–	–	*	–	+	–	–	–	–	–	–	–	–	–	–	–	–
Bt	◆	◆	*	*	◆	◆	◆	◆	◆	◆	◆	◇	◇	◆	◆	◆	◆	◆	◆
Ms	◆	◆	◆	◆	–	(+)	–	◆	◆	◇	◇	◆	◆	(+)	–	–	(+)	–	–
Grt	–	–	+	–	–	*	*	*	*	*	*	*	*	*	–	*	*	+	*
St	–	–	–	–	–	–	–	–	–	–	–	*	*	◇	◆	◆	–	–	–
And	–	–	–	–	–	–	–	*	*	–	*	*	*	+	–	–	–	–	–
Crd	–	–	–	–	–	–	*	–	*	–	*	+	+	+	–	*	–	+	–
Sil	–	–	–	–	–	–	–	–	+	–	–	–	–	+	–	–	–	+	–
Ep	*	*	–	–	*	+	–	–	–	–	–	–	–	–	–	–	–	–	–
Chl	*	(+)	–	+	(+)	–	–	–	–	–	+	–	–	(+)	(+)	(+)	()	–	(+)
Tur	(1)	(1)	+	(1)	+	+	+	+	+	+	+	+	+	+	+	+	+	+	+
Ilm	–	–	–	–	–	–	–	+	+	+	+	+	+	+	+	+	+	+	+
Rt	–	–	–	–	–	–	–	–	–	–	–	–	–	+	–	–	–	–	–
Mag	*	+	*	*	+	+	+	–	–	–	–	–	–	–	–	–	–	–	–
Ap	–	–	–	–	–	–	–	–	+	–	–	–	–	–	–	–	+	–	+
Zr	–	–	+	–	+	–	–	–	–	–	–	–	–	–	–	+	–	+	+

Abbreviations: ◆ = >20 vol.%, ◇ = 20–10 vol.%, * = 10–1 vol.%, + = <1 vol.% – : not recorded, ( ): retrograde, (1): tourmaline concentrates in specific laminae.

The Feiran-Solaf complex is a medium- to high-grade terrane comprising gneiss, migmatized gneiss, metapelitic and metapsammitic schist and calc-silicate rock (El-Gaby and Ahmed 1980; El-Tokhi, 1990; El-Shafei and Kusky, 2003; Abd El-Shakour, 2005). At the extreme northwestern part of the complex, at Gabal Samra (Fig. 1), coarse-grained schists locally contain mm- to cm-sized patches of leucosomes, and melanosomes start to appear. The metamorphic schists contain the near-peak assemblages Qtz + Pl (An_{24-28}) + Bt + Grt ± Crd ± Sil (fibrolite) ± Tur + Ilm + Ap, conforming to the upper-amphibolite facies. Preliminary *P-T* estimates using conventional geothermobarometry yielded 600–670ºC and 4.5 kbar. Similar *P-T* conditions were obtained in the migmatites around the Feiran Oasis (Abd El-Shakour, 2005).

Generally, the metamorphic complexes of the Sinai Peninsula underwent three phases of ductile deformation D1–D3, successively, coinciding with the prograde, the peak and the retrograde *P-T* segments of one cycle of regional metamorphism (Eyal, 1980; Abu El-Enen, 1995; Cosca *et al.*, 1999; Abu El-Enen *et al.*, 2003, 2004). A latest, brittle phase of deformation, D4, is related to large-scale extension and tectonic escape during the late stage of the Pan-African orogeny (Abu El-Enen, 1995; Cosca *et al.*, 1999).

Textural characteristics of tourmaline

Tourmaline was investigated and analysed from four areas in three metamorphic complexes of the Sinai Peninsula (Fig. 1): (1) metapelites from Wadi Kid–Wadi Umm Zariq area; and (2) from the Melhaq volcano-sedimentary association of the Kid complex; (3) metapelites of the Taba complex; and (4) metapsammopelites at Gabal Samra in the Feiran-Solaf complex. Four textural types of accessory tourmaline can be distinguished, three of which are related to specific stages of the tectono-metamorphic evolution:

(1) Tourmaline-1 forms cores, which occur in some of the metamorphic tourmaline neoblasts. They are interpreted as detrital grains, derived from pre-Pan-African basement complex(es), which surrounded the former sedimentary basin.

(2) Tourmaline-2 forms inclusions in garnet, staurolite, cordierite and andalusite porphyroblasts. They presumably crystallized before the metamorphic peak, at the prograde branch of the *P-T* path.

(3) Matrix tourmaline-3 is oriented subparallel to, and enveloped by, the main foliation S_2. Consequently, it was formed pre- and/or syn-D_2, and its growth should have taken place along the prograde *P-T* path up to the metamorphic peak.

(4) Matrix tourmaline-4 has grown post-D_2, because it cross-cuts the S2 foliation. We assume that it crystallized just after the metamorphic peak or at the retrograde *P-T* path.

Although bulk chemical control cannot be ruled out completely, the abundance of tourmaline seems to be inversely correlated with increasing peak metamorphic conditions. Its average content reaches up to 2 vol.% in the southern and central part of the Melhaq volcano-sedimentary association of upper-greenschist to lower-amphibolite facies; it decreases to ~0.5 vol.% in the Kid metapelites of lower-amphibolite facies, and is typically ~0.1 vol.% in the the Taba metapelites and Gabal Samra metapsammopelites of middle to upper-amphibolite facies.

Except for the detrital cores, tourmaline in the Sinai metasediments conforms to the criteria put forward for its metamorphic origin (Henry and Guidotti, 1985; Henry and Dutrow, 1992, 1996; Sperlich *et al.*, 1996; Michailidis *et al.*, 1996): (1) there is no evidence of metasomatism in the investigated rocks, i.e. tourmaline is distributed randomly over all the outcrop and not concentrated along specific shear zones or weakness planes; (2) most of the tourmaline grains are pale in colour and exhibit elongate to acicular forms; (3) tourmaline often displays discontinuous colour and chemical zonation, as discussed below; (4) tourmaline overgrows pre-existing detrital grains; (5) opaque minerals, quartz and biotite form inclusions in some of the tourmaline grains; and (6) matrix tourmaline-3 is wrapped by the main foliation. Tourmaline colours, given in the following paragraphs, relate to the ω direction.

Tourmaline of the Melhaq Formation

The grain size and distribution of tourmaline in the Melhaq Formation are controlled by the lithology of the original protolith, by structure and by grade of metamorphism. Tourmaline does not occur in the metavolcanics, but is restricted to metapelitic and mixed metapelitic/metapyroclastic layers. In the Melhaq Formation, the amount of tourmaline is generally <2 vol.%. However, it constitutes up to 15 vol.% in some mm-thin laminae (~2.5 mm thick) rich in biotite and/or epidote, in the southern and central parts of the formation (Fig. 2*a*). Tourmaline-3 is oriented sub-parallel to the main foliation S2. This indicates that tourmaline has grown pre- to syn-tectonically with respect to D_2. Tourmaline-3 in the southern Melhaq Formation forms euhedral to subhedral, slender prismatic crystals, 0.18−0.45 mm long and 0.06−0.10 mm thick, which display uniform olive-green colour and contain opaque inclusions in their cores. There are even smaller tourmaline needles, just visible with the highest magnification (600×).

With increasing metamorphic grade towards the northern part of the Melhaq Formation, matrix tourmaline becomes more sturdy. Euhedral, prismatic crystals of tourmaline-4 with well developed hexagonal cross sections (Fig. 2*b*), 0.40−0.45 mm long and 0.23−0.37 wide, cut across the main foliation. They exhibit green and bluish-green colours with no colour zonation and contain only a few opaque inclusions. By contrast, fine to very fine-grained tourmaline-2 is included in garnet porphyroblasts.

Tourmaline of the Wadi Kid-Wadi Umm Zariq metapelites

Tourmaline from the metapelites at the Wadi Kid–Wadi Umm Zariq area occurs either as inclusions or as matrix crystals. Porphyroblasts of garnet (Fig. 2*c*), andalusite and cordierite, grown pre- to syn-D_2, contain very fine-grained, long-prismatic tourmaline-2, together with biotite, chlorite, muscovite, quartz and ilmenite. Matrix tourmaline-3 forms pale green, prismatic crystals, which are mostly elongate (0.12−0.42 mm long, 0.05−0.09 mm wide) and less commonly stout (e.g. 0.30 mm to 0.18 mm, 0.15 mm to 0.12 mm). Most grains of matrix tourmaline-3 contain poikiloblastic cores with inclusions of quartz and opaque minerals, succeeded by later-grown, inclusion-free rims (Fig. 2*d*). Matrix tourmaline-3 is wrapped by the regional foliation S_2 indicating pre- to syn-D2 growth. In some cases, matrix tourmaline-3 contains sub-rounded cores of orange-brown (e.g. sample K9) or dark bluish-green (e.g. Sample K14) tourmaline-1, which are overgrown by rims of one or two distinct, green and pale green zones, respectively. This texture has been ascribed to secondary growth of metamorphic tourmaline on detrital tourmaline fragments (Zen, 1981). Post-D_2 tourmaline-4 crystals, crosscutting the main S_2 foliation, are rarely observed.

Tourmaline of the Taba metapelites

In the Taba metapelites, tourmaline is rare. In pre- to early-D_2 porphyroblasts of staurolite (Fig. 2*f*) and pinitized cordierite, tiny (0.1 mm), pale green tourmaline-2 inclusions occur, together with muscovite, biotite, chlorite, quartz and ilmenite. Occasionally, they overgrow pale brownish-green

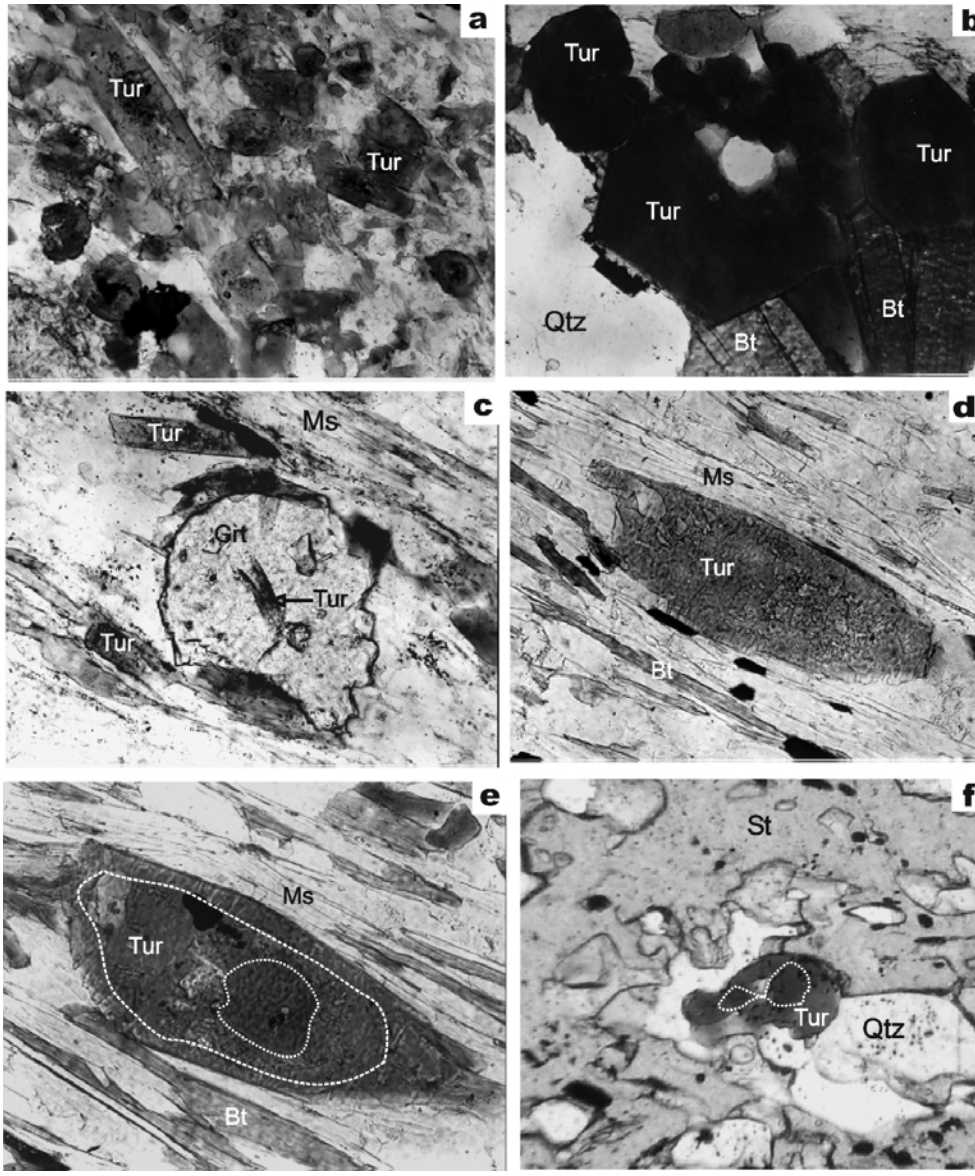

FIG. 2. Photomicrographs in plane polarized light showing typical textural occurrences of tourmaline. (*a*) Tourmaline within biotite and epidote-rich laminae in a meta-calcpelite of the Melhaq volcano-sedimentary association, showing their long prismatic habit, opaque inclusions at their cores and inclusion-free rims. Sample M28; field of view = 0.42 mm wide. (*b*) Euhedral to subhedral tourmaline grains in a high-grade metapelite of the northern Melhaq volcano-sedimentary association crosscuting the main foliation, thus manifesting growth as a retrograde phase. Sample M50; field of view = 0.35 mm wide. (*c*) Prograde tourmaline inclusion in garnet and peak matrix tourmalines in a metapelite from Wadi Kid–Wadi Umm Zariq. Sample K3; field of view = 0.58 mm wide. (*d*) Peak tourmaline with a core containing inclusions of quartz and fine opaque dust in a metapelite from Wadi Kid–Wadi Umm Zariq. Sample K9; field of view = 0.15 mm wide. (*e*) Sub-rounded grain of detrital tourmaline surrounded by inner and outer rims, Sample K9; field of view = 0.13 mm wide. (*f*) Small, anhedral grain of detrital tourmaline, overgrown by prograde tourmaline, included in a staurolite poikiloblast in a metapelite from the Taba complex. Sample T3; field of view = 0.30 mm wide.

cores of detrital tourmaline-1 (Fig. 2*f*). Matrix tourmaline-3 forms green, subhedral crystals of elongate shape (0.10–0.12 mm long, 0.07–0.08 wide), which lack visible colour zoning. They are oriented parallel to the main foliation (S_2).

Tourmaline of the Gabal Samra metapsammopelites

Scarce matrix tourmaline-3 from the metapsammopelites at Gabal Samra forms euhedral, prismatic crystals (0.84–1.75 mm long, 0.32–0.70 wide) with pyramidal terminations, which are oriented sub-parallel to the main foliation. They are pale yellowish-brown to colourless, lacking colour zonation or cores of detrital tourmaline-1. Commonly, matrix tourmaline exhibits poikiloblastic texture with inclusions of biotite and quartz.

Chemical composition of tourmaline

Analytical techniques

Because of the tiny to fine-grained size and the scarcity of tourmaline in the Sinai metasediments, only microprobe analyses were performed in this study, thus not allowing us to analyse Fe_2O_3/FeO, Li_2O, B_2O_3 and H_2O. Electron microprobe (EMP) analyses were carried out on a CAMECA SX 50 instrument with three independent WDS channels at the Institute of Mineralogy, Würzburg University, Germany. Analytical conditions were 15 kV accelerating voltage, 15 nA beam current and 1–2 μm beam diameter. Well characterized natural oxides, silicates and synthetic mineral standards supplied by CAMECA were used for reference, and the data were fully corrected using the PAP programme of CAMECA. The detection limits of the individual oxides are ~0.05 to 0.10 wt.%; errors are <1% relative for major elements, 2% relative for Na_2O, and <5% relative for minor elements.

A total of 244 spot analyses were carried out in 19 samples (some with two thin sections) representing the tourmaline-bearing metapelitic, metapsammopelitic, and calc-metapelitic rocks from the three metamorphic complexes. To obtain information on compositional zoning, spot analyses were performed in some of the mineral grains along traverses, roughly parallel, in a few cases also perpendicular, to the *c* axes; otherwise core-rim analyses were taken.

The structural formulae of tourmaline $XY_3Z_6T_6O_{18}(BO_3)_3V_3W$ (Hawthorne and Henry, 1999) were calculated by normalizing to 31 (O + OH + F) and 15 cations in the tetrahedral and octahedral sites (T+Z+Y). B_2O_3 contents were estimated by stoichiometrical iteration, assuming B = 3 in the structural formula (Henry and Guidotti 1985; Dutrow *et al.*, 1999). An admittedly rough estimate of Fe^{3+} and Fe^{2+} was made by charge balance, whereby the negative charges are calculated by using the empirical formula OH = 3+(1-F)/2 and O = 31–(F+OH) of Grice and Ercit (1993). Following the suggestions of these authors, we filled deficits in the T site with Ti and, if necessary, with $Al^{[4]}$. The Z position contains $Al^{[6]}$, Cr and some Fe^{3+} up to a total of six cations, while the Y position is filled by Mg, Mn, Fe^{2+} and most of the Fe^{3+} as well as some remaining $Al^{[6]}$, Cr and Ti. The possible Li content can be estimated approximately by difference, in cases where the sum of the Y cations is <3 (see below). Selected EMP analyses of tourmaline are presented in Table 2; calculated end-members for the textural types of tourmaline are summarized in Table 3.

Analytical results

In all samples investigated, tourmaline belongs to the alkali-tourmaline group of Hawthorne and Henry (1999), as they have 0.50–0.81 Na+K a.p.f.u., 0.01–0.41 Ca a.p.f.u. and 0.03–0.50 X-site vacancies □ p.f.u. (Fig. 3). The tetrahedral site contains 0.00–0.21 $Al^{[4]}$, if Ti is placed in the T position. In general, the Z site is completely filled by Al (+ Cr) but, in a few cases, some Fe^{3+} (up to 0.66 a.p.f.u.) was added to attain the ideal sum of Z = 6. Most of the Y site is occupied by Fe^{2+}, Fe^{3+} and Mg with minor Ti, Al, Cr and Mn. The sum of these Y cations is generally <3. Assuming that this deficiency is due to the presence of a small amount of Li, which can be roughly estimated as $Li = 3-\Sigma(Ti+Al^{[6]}+Cr+Fe+Mg+Mn)_Y$, we arrive at up to 0.24 Li a.p.f.u.

As shown in the Ca/(Ca+Na) and □/(Na+□) *vs.* Mg/(Mg+Fe) diagrams (Fig. 4) and the $Al-Al_{50}Fe^{tot}{}_{50}-Al_{50}Mg_{50}$ triangle (Fig. 5), the tourmaline investigated belongs to the schorl–dravite$_{ss}$ group with minor amounts of feruvite/uvite and foitite/Mg-foitite (*cf.* Table 3). From the substitutions known to occur in tourmaline, five types were established in the tourmaline investigated (Table 2): (1) $^{Y}Mg \rightleftharpoons {}^{Y}Fe^{2+}$; (2) Tschermak's substitution $^{Y}(Mg,Fe^{2+},Mn^{2+}) + {}^{T}Si \rightleftharpoons {}^{Y}(Al^{[6]},Fe^{3+},Cr^{3+}) + {}^{T}Al^{[4]}$ as indicated by the deficiency in Si and the fact that Al^{tot} is generally >6 a.p.f.u.; (3) $^{X}Na + {}^{Y}(Al^{[6]},Fe^{3+},Cr^{3+})$

TABLE 2. Representative microprobe analyses (wt.%) of tourmalines from Sinai metasediments.

Area	Melhaq												Wadi Kid–W. Umm Zariq								
Sample no.	– M28 –		– M34 –		M38	M43	– M46 –		M47	—— M50 ——			– K6 –		K9				K14		
Position	(c)		(c)		(c)	(c)	(c)		(d)	(b) – in Grt		(d)	(c)		(a)	(b)	(c)		(a)	(b)	(c)
	rim	core	rim	core			rim	core		rim	core		rim	core	detrital	in crd.	rim	core	detrital	in grt	rim
SiO_2	35.88	35.91	35.23	35.49	35.15	35.25	35.17	35.05	34.60	35.49	35.51	34.84	35.37	36.25	34.92	35.70	34.59	35.23	34.22	35.11	36.04
TiO_2	0.47	0.06	0.04	0.18	0.66	0.05	0.69	0.80	0.36	0.64	0.46	0.40	0.77	0.31	1.89	0.71	0.59	0.77	0.06	0.83	0.26
B_2O_3*	10.52	10.47	10.55	10.52	10.41	10.45	10.57	10.52	10.43	10.53	10.44	10.47	10.61	10.69	10.51	10.54	10.37	10.52	10.00	10.44	10.63
Al_2O_3	30.81	31.00	31.41	30.89	30.73	31.27	32.11	31.49	33.22	32.23	31.80	33.11	33.40	33.82	31.03	32.87	32.12	33.19	27.33	32.09	33.80
Cr_2O_3	0.01	0.00	0.00	0.02	0.00	0.04	0.07	0.07	0.00	0.02	0.01	0.02	0.02	0.03	0.09	0.02	0.04	0.04	0.02	0.04	0.04
MgO	6.56	5.98	7.74	7.39	6.11	7.14	7.18	7.09	4.68	5.87	5.50	4.76	6.20	5.72	7.13	5.35	5.55	5.46	4.64	5.26	4.92
CaO	0.35	0.11	1.67	1.47	0.07	1.37	1.55	1.58	0.68	0.68	0.46	0.91	0.77	0.10	1.89	0.13	0.92	0.80	1.71	1.10	0.08
MnO	0.04	0.00	0.09	0.04	0.00	0.12	0.02	0.05	0.09	0.11	0.20	0.05	0.00	0.02	0.09	0.13	0.00	0.07	0.09	0.17	0.00
Fe_2O_3*	4.79	5.25	5.04	5.15	5.07	4.49	3.68	4.15	4.16	4.08	3.98	3.85	4.30	4.20	3.07	4.05	4.08	3.69	5.32	3.85	3.78
FeO*	5.29	5.93	4.04	4.02	5.75	4.34	4.65	4.33	6.74	5.56	6.46	6.85	3.35	3.54	4.77	5.21	5.75	5.27	10.31	5.93	4.71
Li_2O*	0.09	0.01	0.00	0.11	0.06	0.08	0.07	0.15	0.05	0.10	0.00	0.11	0.24	0.30	0.18	0.13	0.11	0.11	0.05	0.17	0.37
Na_2O	2.51	2.36	1.64	1.67	2.69	1.81	1.75	1.72	1.84	2.03	2.03	1.85	1.73	2.28	1.47	2.08	1.85	1.60	1.79	1.54	2.54
K_2O	0.03	0.00	0.02	0.04	0.00	0.07	0.09	0.06	0.06	0.01	0.00	0.06	0.07	0.02	0.05	0.01	0.03	0.02	0.04	0.02	0.01
F	0.20	0.21	0.16	0.27	0.23	0.14	0.00	0.15	0.07	0.09	0.00	0.07	0.24	0.27	0.00	0.11	0.11	0.04	0.28	0.12	0.27
H_2O*	3.13	3.11	3.15	3.11	3.09	3.12	3.19	3.14	3.13	3.16	3.15	3.15	3.15	3.16	3.17	3.16	3.11	3.17	2.95	3.12	3.14
Total	100.67	100.40	100.77	100.37	100.01	99.75	100.79	100.35	100.11	100.60	100.00	100.49	100.21	100.71	100.25	100.20	99.21	99.98	98.81	99.79	100.59
- O~F	0.08	0.09	0.07	0.11	0.09	0.06	0.00	0.06	0.03	0.04	0.00	0.03	0.10	0.11	0.00	0.05	0.05	0.02	0.12	0.05	0.11
Total	100.59	100.31	100.70	100.25	99.92	99.69	100.79	100.28	100.08	100.56	100.00	100.46	100.11	100.60	100.25	100.16	99.17	99.96	98.69	99.73	100.48
Structural formulae																					
Si	5.930	5.961	5.804	5.866	5.869	5.861	5.782	5.792	5.765	5.856	5.913	5.782	5.794	5.896	5.776	5.887	5.797	5.822	5.948	5.847	5.895
Ti	0.058	0.007	0.005	0.022	0.083	0.006	0.085	0.099	0.045	0.079	0.058	0.050	0.095	0.038	0.224	0.088	0.074	0.096	0.008	0.104	0.032
Al	0.011	0.032	0.191	0.112	0.048	0.133	0.132	0.109	0.190	0.064	0.029	0.168	0.111	0.066	0.000	0.025	0.129	0.082	0.044	0.049	0.073
Total T	6.000	6.000	6.000	6.000	6.000	6.000	6.000	6.000	6.000	6.000	6.000	6.000	6.000	6.000	6.000	6.000	6.000	6.000	6.000	6.000	6.000
B*	3.000	3.000	3.000	3.000	3.000	3.000	3.000	3.000	3.000	3.000	3.000	3.000	3.000	3.000	3.000	3.000	3.000	3.000	3.000	3.000	3.000
Al	5.990	6.000	5.908	5.905	5.998	5.994	6.000	6.000	6.000	6.000	6.000	6.000	6.000	6.000	6.000	6.000	6.000	6.000	5.555	6.000	6.000
Cr	0.001	0.000	0.000	0.003	0.000	0.005	0.000	0.000	0.000	0.000	0.000	0.000	0.000	0.000	0.000	0.000	0.000	0.000	0.003	0.000	0.000
Fe^{3+}*	0.009	0.000	0.092	0.093	0.002	0.001	0.000	0.000	0.000	0.000	0.000	0.000	0.000	0.000	0.000	0.000	0.000	0.000	0.443	0.000	0.000
Total *Z*	6.000	6.000	6.000	6.000	6.000	6.000	6.000	6.000	6.000	6.000	6.000	6.000	6.000	6.000	6.000	6.000	6.000	6.000	6.000	6.000	6.000
Al	0.000	0.032	0.000	0.000	0.000	0.000	0.089	0.023	0.334	0.203	0.211	0.309	0.338	0.416	0.049	0.362	0.215	0.381	0.000	0.249	0.442
Ti	0.000	0.000	0.000	0.000	0.000	0.000	0.000	0.000	0.000	0.000	0.000	0.000	0.000	0.000	0.012	0.000	0.000	0.000	0.000	0.000	0.000
Cr	0.000	0.000	0.000	0.000	0.000	0.000	0.009	0.009	0.000	0.003	0.001	0.003	0.003	0.004	0.012	0.003	0.005	0.005	0.000	0.005	0.005
Fe^{3+}*	0.586	0.656	0.532	0.548	0.635	0.561	0.456	0.516	0.522	0.507	0.499	0.481	0.530	0.514	0.382	0.503	0.514	0.458	0.253	0.482	0.465
Fe^{2+}*	0.732	0.823	0.556	0.556	0.803	0.603	0.639	0.598	0.939	0.767	0.899	0.950	0.459	0.482	0.659	0.719	0.806	0.729	1.499	0.825	0.644
Mg	1.616	1.480	1.901	1.821	1.521	1.770	1.760	1.747	1.163	1.444	1.365	1.178	1.514	1.387	0.118	1.315	1.387	1.345	1.202	1.306	1.200

Mn	0.004	0.000	0.010	0.004	0.000	0.014	0.003	0.006	0.010	0.013	0.023	0.006	0.000	0.003	1.758	0.015	0.000	0.008	0.010	0.020	0.000
Li*	0.062	0.010	0.001	0.071	0.042	0.052	0.044	0.102	0.034	0.064	0.001	0.074	0.156	0.195	0.010	0.083	0.073	0.073	0.035	0.113	0.244
Total *Y*	3.000	3.000	3.000	3.000	3.000	3.000	3.000	3.000	3.000	3.000	3.000	3.000	3.000	3.000	3.000	3.000	3.000	3.000	3.000	3.000	3.000
Ca	0.062	0.020	0.295	0.260	0.013	0.244	0.273	0.280	0.121	0.120	0.082	0.162	0.135	0.017	0.335	0.023	0.165	0.142	0.318	0.196	0.014
Na	0.804	0.759	0.524	0.535	0.871	0.583	0.558	0.551	0.594	0.649	0.655	0.595	0.549	0.719	0.471	0.665	0.601	0.513	0.603	0.497	0.805
K	0.006	0.000	0.004	0.008	0.000	0.015	0.019	0.013	0.013	0.002	0.000	0.013	0.015	0.004	0.011	0.002	0.006	0.004	0.009	0.004	0.002
Vac	0.127	0.221	0.177	0.196	0.117	0.158	0.150	0.157	0.271	0.228	0.263	0.230	0.301	0.260	0.183	0.310	0.227	0.342	0.069	0.302	0.178
Total *X*	1.000	1.000	1.000	1.000	1.000	1.000	1.000	1.000	1.000	1.000	1.000	1.000	1.000	1.000	1.000	1.000	1.000	1.000	1.000	1.000	1.000
F	0.105	0.110	0.083	0.141	0.119	0.076	0.000	0.078	0.037	0.000	0.037	0.047	0.124	0.139	0.000	0.057	0.058	0.021	0.154	0.063	0.140
OH*	3.448	3.445	3.450	3.429	3.441	3.462	3.500	3.461	3.482	3.500	3.482	3.477	3.438	3.431	3.500	3.471	3.471	3.490	3.427	3.468	3.430
Mg/ (Fe+Mg)	0.549	0.500	0.617	0.603	0.514	0.603	0.617	0.611	0.443	0.531	0.494	0.451	0.605	0.582	0.628	0.518	0.512	0.531	0.354	0.500	0.520

Area	Wadi Kid–W. Umm Zariq								Taba								Gabal Samra			
Sample no.	K22		K25			K35			T2		T3		T10		T12		Z1		Z3	
Position	(b) in grt	(c) rim	(b) core	(c) in and		(c) in grt	(b) rim	(c) core	(a) in st	(b)	(b) detrital	(c) in st	(b) in st	(b) in crd	rim	core	rim	core	rim	core
SiO_2	34.40	35.43	35.91	35.03	35.55	35.87	35.17	35.10	35.36	34.27	35.27	35.85	34.50	34.86	35.58	35.36	35.45	35.23	35.86	35.08
TiO_2	0.79	0.80	0.17	0.81	0.78	0.80	0.91	0.86	0.82	1.50	1.14	0.89	0.81	1.19	0.93	0.83	1.08	1.35	0.90	0.94
B_2O_3*	10.39	10.548	10.47	10.57	10.50	10.47	10.58	10.49	10.57	10.44	10.57	10.69	10.54	10.51	10.65	10.65	10.61	10.61	10.77	10.66
Al_2O_3	32.29	33.180	33.12	34.19	32.39	31.73	32.87	32.84	32.84	33.22	32.12	33.31	35.04	33.13	33.66	33.96	32.98	33.29	33.58	33.96
Cr_2O_3	0.03	0.080	0.03	0.03	0.09	0.01	0.03	0.03	0.03	0.10	0.06	0.00	0.00	0.04	0.10	0.18	0.04	0.09	0.06	0.08
MgO	5.61	5.970	4.34	5.16	5.50	4.99	5.76	5.58	6.30	5.49	6.30	6.08	4.32	5.53	6.62	6.51	6.76	6.60	7.49	6.91
CaO	0.83	0.700	0.28	0.69	0.96	0.39	0.98	0.87	0.57	1.01	1.07	0.92	0.97	1.14	0.73	0.80	1.15	0.86	0.90	0.95
MnO	0.12	0.000	0.04	0.06	0.07	0.06	0.05	0.10	0.06	0.00	0.06	0.06	0.04	0.09	0.12	0.07	0.07	0.04	0.07	0.07
Fe_2O_3*	4.76	3.634	3.55	3.69	3.44	4.24	4.29	3.81	4.69	3.36	4.71	3.79	3.65	3.29	3.56	3.84	3.39	3.32	4.03	3.68
FeO*	4.59	4.030	6.84	5.38	5.92	5.59	4.69	4.95	3.14	5.10	3.98	4.53	5.16	5.09	2.84	2.72	3.18	2.98	1.95	2.76
Li_2O*	0.17	0.204	0.08	0.07	0.11	0.29	0.23	0.17	0.22	0.12	0.23	0.17	0.25	0.21	0.23	0.21	0.27	0.28	0.22	0.18
Na_2O	1.72	1.800	1.72	1.55	1.56	1.92	1.74	1.65	1.81	1.47	1.56	1.65	1.35	1.62	1.87	1.71	1.78	1.91	1.92	1.90
K_2O	0.01	0.020	0.01	0.00	0.02	0.07	0.04	0.03	0.01	0.01	0.05	0.08	0.01	0.00	0.07	0.03	0.03	0.06	0.01	0.05
F	0.27	0.110	0.00	0.00	0.00	0.28	0.23	0.11	0.29	0.00	0.30	0.10	0.15	0.06	0.11	0.14	0.12	0.12	0.17	0.09
H_2O*	3.07	3.158	3.16	3.19	3.17	3.10	3.14	3.14	3.12	3.15	3.12	3.20	3.15	3.16	3.19	3.18	3.17	3.17	3.21	3.20
Total	99.06	99.664	99.72	100.42	100.05	99.81	100.70	99.73	99.83	99.23	100.55	101.32	99.93	99.91	100.26	100.20	100.09	99.91	101.14	100.51
- O~F	0.11	0.046	0.00	0.00	0.00	0.12	0.10	0.05	0.12	0.00	0.13	0.04	0.06	0.03	0.05	0.06	0.05	0.05	0.07	0.04
Total	98.94	99.618	99.72	100.42	100.05	99.69	100.60	99.68	99.70	99.23	100.42	101.28	99.87	99.89	100.21	100.14	100.04	99.86	101.07	100.48

TABLE 2 (*contd.*)

Area	Wadi Kid–W. Umm Zariq								Taba								Gabal Samra			
Sample no.	K22			K25		K35			T2		T3		T10		T12		Z1		Z3	
Position	(b) in grt	(c) rim	(b) core	(c) in and		(c) in grt	(b) rim	(c) core	(a) in st	(b)	(b) detrital	(c) in st	(b) in st	(b) in crd	rim	core	rim	core	rim	core
Structural formulae																				
Si	5.757	5.839	5.964	5.760	5.886	5.954	5.779	5.815	5.817	5.707	5.797	5.831	5.691	5.765	5.805	5.771	5.807	5.774	5.789	5.718
Ti	0.099	0.099	0.021	0.100	0.097	0.046	0.112	0.107	0.101	0.188	0.141	0.109	0.100	0.148	0.114	0.102	0.133	0.166	0.109	0.115
Al	0.144	0.062	0.015	0.140	0.017	0.000	0.109	0.077	0.081	0.105	0.062	0.060	0.208	0.087	0.081	0.127	0.060	0.060	0.101	0.167
Total *T*	6.000	6.000	6.000	6.000	6.000	6.000	6.000	6.000	6.000	6.000	6.000	6.000	6.000	6.000	6.000	6.000	6.000	6.000	6.000	6.000
B*	3.000	3.000	3.000	3.000	3.000	3.000	3.000	3.000	3.000	3.000	3.000	3.000	3.000	3.000	3.000	3.000	3.000	3.000	3.000	3.000
Al	6.000	6.000	6.000	6.000	6.000	6.000	6.000	6.000	6.000	6.000	6.000	6.000	6.000	6.000	6.000	6.000	6.000	6.000	6.000	6.000
Cr	0.000	0.000	0.000	0.000	0.000	0.000	0.000	0.000	0.000	0.000	0.000	0.000	0.000	0.000	0.000	0.000	0.000	0.000	0.000	0.000
Fe^{3+}*	0.000	0.000	0.000	0.000	0.000	0.000	0.000	0.000	0.000	0.000	0.000	0.000	0.000	0.000	0.000	0.000	0.000	0.000	0.000	0.000
Total *Z*	6.000	6.000	6.000	6.000	6.000	6.000	6.000	6.000	6.000	6.000	6.000	6.000	6.000	6.000	6.000	6.000	6.000	6.000	6.000	6.000
Al	0.225	0.382	0.467	0.485	0.303	0.207	0.256	0.335	0.286	0.414	0.160	0.326	0.604	0.371	0.391	0.405	0.307	0.370	0.287	0.357
Ti	0.000	0.000	0.000	0.000	0.000	0.054	0.000	0.000	0.000	0.000	0.000	0.000	0.000	0.000	0.000	0.000	0.000	0.000	0.000	0.000
Cr	0.004	0.010	0.004	0.004	0.012	0.001	0.004	0.004	0.004	0.013	0.008	0.000	0.000	0.005	0.013	0.023	0.005	0.012	0.008	0.010
Fe^{3+}*	0.600	0.451	0.444	0.457	0.428	0.530	0.530	0.476	0.581	0.421	0.583	0.464	0.453	0.409	0.437	0.472	0.418	0.410	0.489	0.452
Fe^{2+}*	0.643	0.555	0.950	0.739	0.819	0.776	0.644	0.685	0.432	0.710	0.547	0.616	0.712	0.704	0.387	0.371	0.436	0.409	0.264	0.376
Mg	0.115	0.135	0.056	1.265	1.358	1.235	1.411	1.378	0.145	1.363	0.151	0.113	1.062	1.363	1.610	1.584	1.651	1.613	1.803	1.679
Mn	1.400	1.467	1.075	0.007	0.008	0.007	0.006	0.011	1.545	0.000	1.544	1.474	0.004	0.010	0.014	0.008	0.008	0.004	0.008	0.008
Li*	0.014	0.000	0.004	0.043	0.072	0.190	0.149	0.111	0.007	0.079	0.007	0.007	0.164	0.138	0.149	0.136	0.176	0.184	0.141	0.118
Total *Y*	3.000	3.000	3.000	3.000	3.000	3.000	3.000	3.000	3.000	3.000	3.000	3.000	3.000	3.000	3.000	3.000	3.000	3.000	3.000	3.000
Ca	0.149	0.124	0.050	0.122	0.170	0.069	0.173	0.154	0.100	0.180	0.188	0.160	0.171	0.202	0.128	0.140	0.202	0.151	0.156	0.166
Na	0.558	0.575	0.554	0.494	0.501	0.618	0.554	0.530	0.577	0.475	0.497	0.520	0.432	0.519	0.591	0.541	0.565	0.607	0.601	0.600
K	0.002	0.004	0.002	0.000	0.004	0.015	0.008	0.006	0.002	0.002	0.010	0.017	0.002	0.000	0.015	0.006	0.006	0.013	0.002	0.010
Vac	0.291	0.297	0.394	0.384	0.325	0.298	0.265	0.309	0.320	0.343	0.304	0.303	0.395	0.279	0.266	0.313	0.227	0.230	0.241	0.223
Total *X*	1.000	1.000	1.000	1.000	1.000	1.000	1.000	1.000	1.000	1.000	1.000	1.000	1.000	1.000	1.000	1.000	1.000	1.000	1.000	1.000
F	0.143	0.057	0.000	0.000	0.000	0.147	0.119	0.058	0.151	0.000	0.156	0.051	0.078	0.031	0.057	0.072	0.062	0.062	0.087	0.046
OH*	3.429	3.471	3.500	3.500	3.500	3.427	3.440	3.471	3.425	3.500	3.422	3.474	3.461	3.484	3.472	3.464	3.469	3.469	3.457	3.477
Mg/(Fe+Mg)	0.530	0.593	0.435	0.514	0.521	0.486	0.546	0.543	0.604	0.547	0.577	0.577	0.477	0.551	0.661	0.653	0.659	0.663	0.705	0.670

Abbreviations: (a): Detrital (tourmaline-1) (b): Prograde (tourmaline-2), (c): Peak (tourmaline-3), (d): Post-peak (Tourmaline-4), * = calculated

TABLE 3. End-member composition and X_{Mg} range of tourmalines from Sinai metasediments.

Metamorphic area	End-member composition	X_{Mg}
Melhaq		
	Prograde ($dravite_{32-38}$ $schorl_{31-37}$ $uvite_{2-6}$ $feruvite_{2-6}$ Mg−$foitite_{10-13}$ $foitite_{10-13}$)	0.49−0.53
	Peak ($dravite_{25-45}$ $schorl_{19-42}$ $uvite_{1-24}$ $feruvite_{1-17}$ Mg−$foitite_{2-16}$ $foitite_{1-18}$)	0.55−0.64
	Retrograde ($dravite_{27-31}$ $schorl_{32-35}$ $uvite_{5-8}$ $feruvite_{9-7}$ Mg−$foitite_{10-12}$ $foitite_{11-15}$)	0.44−0.47
W. Kid–W. Umm Zariq		
	Detrital-1 ($dravite_{20-23}$ $schorl_{36-42}$ $uvite_{10-11}$ $feruvite_{17-22}$ Mg−$foitite_{2-5}$ $foitite_{3-9}$)	0.33−0.38
	Detrital-2 ($dravite_{30-34}$ $schorl_{18-20}$ $uvite_{21-24}$ $feruvite_{12-13}$ Mg−$foitite_{6-11}$ $foitite_{4-7}$)	0.63−0.64
	Prograde ($dravite_{24-32}$ $schorl_{24-33}$ $uvite_{2-10}$ $feruvite_{2-10}$ Mg−$foitite_{14-20}$ $foitite_{14-20}$)	0.43−0.58
	Peak ($dravite_{26-42}$ $schorl_{20-40}$ $uvite_{1-13}$ $feruvite_{1-10}$ Mg−$foitite_{9-26}$ $foitite_{9-23}$)	0.45−0.61
Taba		
	Detrital-2 ($dravite_{29-31}$ $schorl_{21-26}$ $uvite_{7-11}$ $feruvite_{5-8}$ Mg−$foitite_{17-18}$ $foitite_{13-14}$)	0.55−0.58
	Prograde ($dravite_{21-31}$ $schorl_{21-26}$ $uvite_{6-11}$ $feruvite_{5-9}$ Mg−$foitite_{15-25}$ $foitite_{13-23}$)	0.48−0.60
	Peak ($dravite_{33-40}$ $schorl_{19-27}$ $uvite_{3-9}$ $feruvite_{2-5}$ Mg−$foitite_{18-22}$ $foitite_{13-16}$)	0.55−0.66
G. Samra		
	Peak-retrograde ($dravite_{31-55}$ $schorl_{16-24}$ $uvite_{8-15}$ $feruvite_{4-9}$ Mg−$foitite_{7-26}$ $foitite_{3-14}$)	0.63−0.73

Detrital-1: bluish-green tourmaline, Detrital-2: Orange-brown tourmaline

$\rightleftharpoons {}^{X}Ca+{}^{Y}(Mg,Fe^{2+},Mn^{2+})$; (4) $2\,{}^{X}Na \rightleftharpoons {}^{X}Ca+{}^{X}\square$; and (5) ${}^{X}Na+{}^{Y}(Mg,Fe^{2+}) \rightleftharpoons {}^{X}\square+{}^{Y}(Al,Fe^{3+},Cr)$.

Most of the tourmaline analyses revealed low Ca values of 0.02−0.24 a.p.f.u., high Al values of 6.0−6.8 a.p.f.u. and X_{Mg} values of 0.42−0.73. Higher Ca (up to 0.4 a.p.f.u.) and lower Al (down to 5.7 a.p.f.u.) values are restricted to some tourmaline coexisting with epidote in schists of the Melhaq Formation (Fig. 6*a*,*b*). Cr_2O_3, MnO and K_2O are generally at or below the detection limit; exceptional values are 0.25 wt.% MnO and 0.33 wt.% K_2O in tourmaline of samples T2 and Z1, respectively.

Tourmaline cores in samples K14, K9 and T3, interpreted as detrital grains, form three distinct groups. In sample K14, they are richer in Fe than

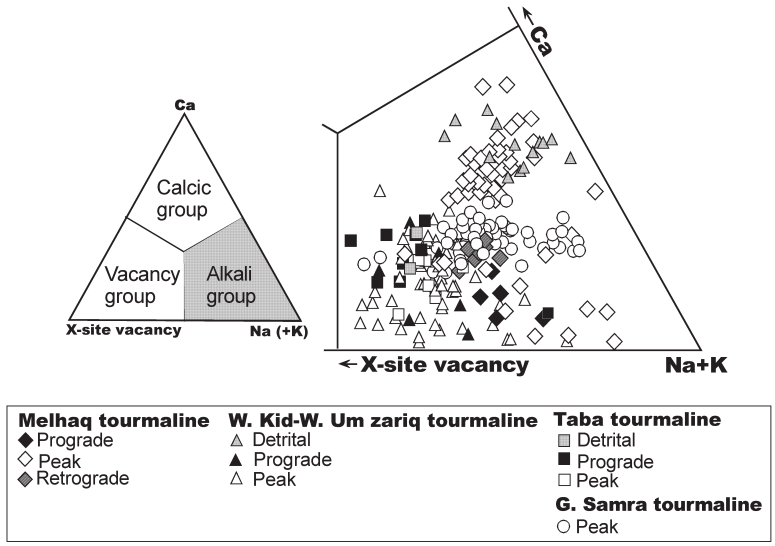

FIG. 3. Different textural generations of tourmaline from Sinai metasediments plotted in the classification triangle for the principal groups of tourmaline based on *X*-site occupancy (Hawthorne and Henry, 1999).

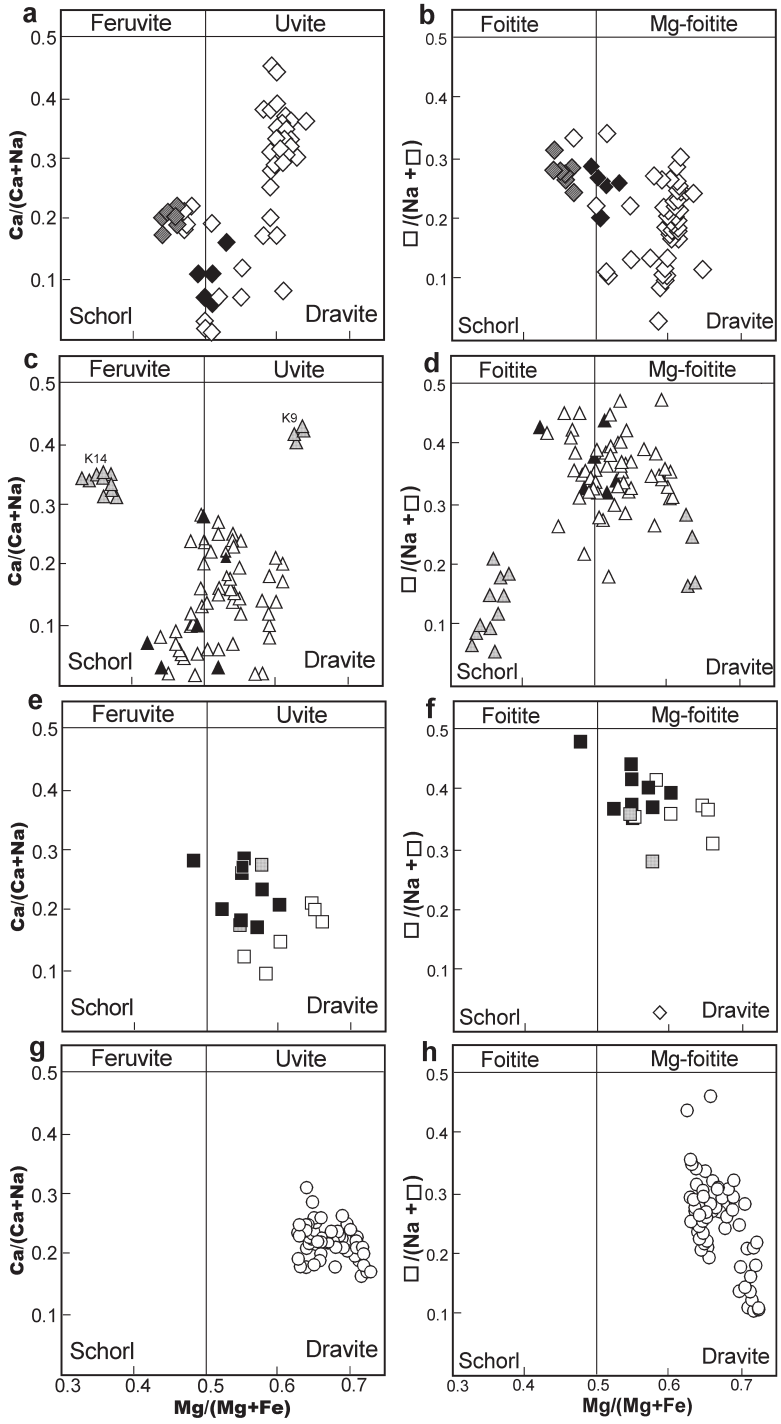

FIG. 4. Plots of investigated tourmaline in the Ca/(Ca+Na) *vs.* Mg/(Mg+Fe^{tot}) and in the □/(Na+□) *vs.* Mg/(Mg+Fe^{tot}) diagrams; (*a,b*) Melhaq tourmaline; (*c,d*) Wadi Kid−Umm Zariq tourmaline; (*e,f*) Taba tourmaline; and (*g,h*) G. Samra tourmaline. Symbols as in Fig. 3.

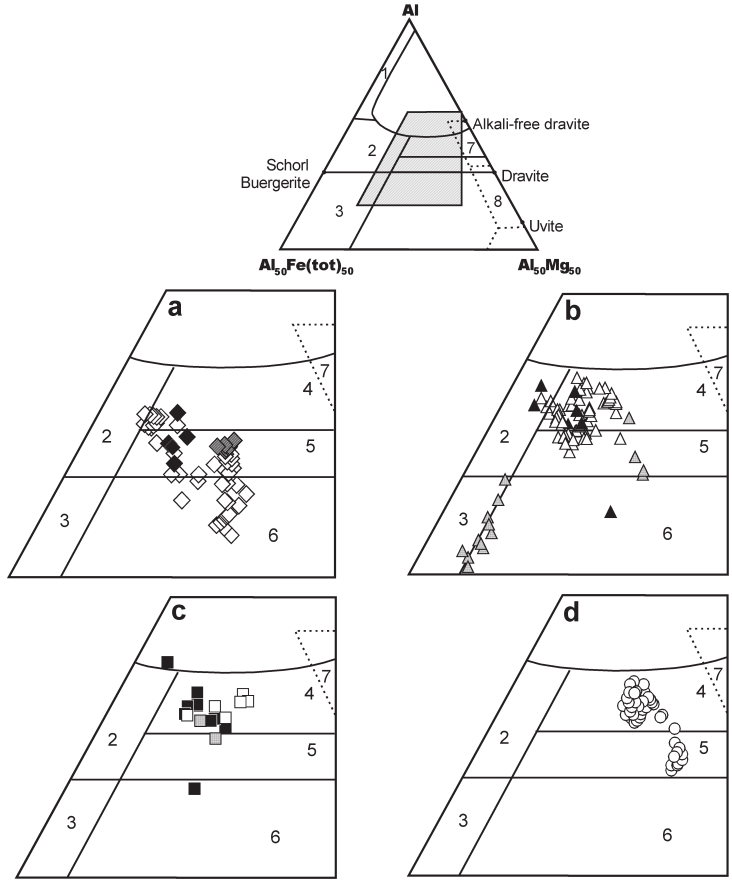

FIG. 5. Al-Fe^{tot}-Mg ternary diagram (in molecular proportions) for tourmaline from Sinai metasediments: (*a*) Melhaq tourmaline; (*b*) Wadi-Kid−Um Zariq tourmaline; (*c*) Taba tourmaline; and (*d*) G. Samra tourmalines. The fields, defined by Henry and Guidotti (1985), represent the composition of: (1) Li-rich granitoids, pegmatites and aplites; (2) Li-poor granitoids and their associated pegmatites and aplites; (3) Fe^{3+}-rich quartz-tourmaline rocks (hydrothermally altered granite); (4) metapelites and metapsammites coexisting with an Al-saturating phase; (5) metapelites and metapsammites not coexisting with an Al-saturating phase; (6) Fe^{3+}-rich quartz-tourmaline rocks, calc-silicate rocks, and metapelites; (7) low-Ca meta-ultramafics and Cr-, V-rich metasediments; and (8) metacarbonates and metapyroxenite. Symbols as in Fig. 3.

the surrounding tourmaline-3 with X_{Mg} values of 0.34−0.38 and have Ca contents of 0.27−0.33 a.p.f.u. (Fig. 6*c*). In contrast, a detrital tourmaline core in sample K9 yielded higher X_{Mg} values of 0.63−064 than the including tourmaline-3 and has 0.34−0.37 a.p.f.u. Ca (Fig. 6c). On the other hand, detrital tourmaline of sample T3 yielded an X_{Mg} value of 0.58 similar to that of surrounding tourmaline-2 (Fig. 6*e*,*f*). End-member compositions and X_{Mg} values of tourmalines from the metamorphic areas investigated, and in different textural positions, are summarized in Table 3.

Chemical zoning

Microprobe analyses across traverses, oriented roughly parallel to the *c* axes of some tourmaline grains, show two different types of element distribution.

The first type, characterized by a slight compositional polarity (cf. Sperlich, 1990; Henry and Dutrow 1992; Sperlich *et al.*, 1996), was recorded in tourmaline-4 from the northern part of the Melhaq Formation (sample M46). It displays a small, continuous increase in Al, and a

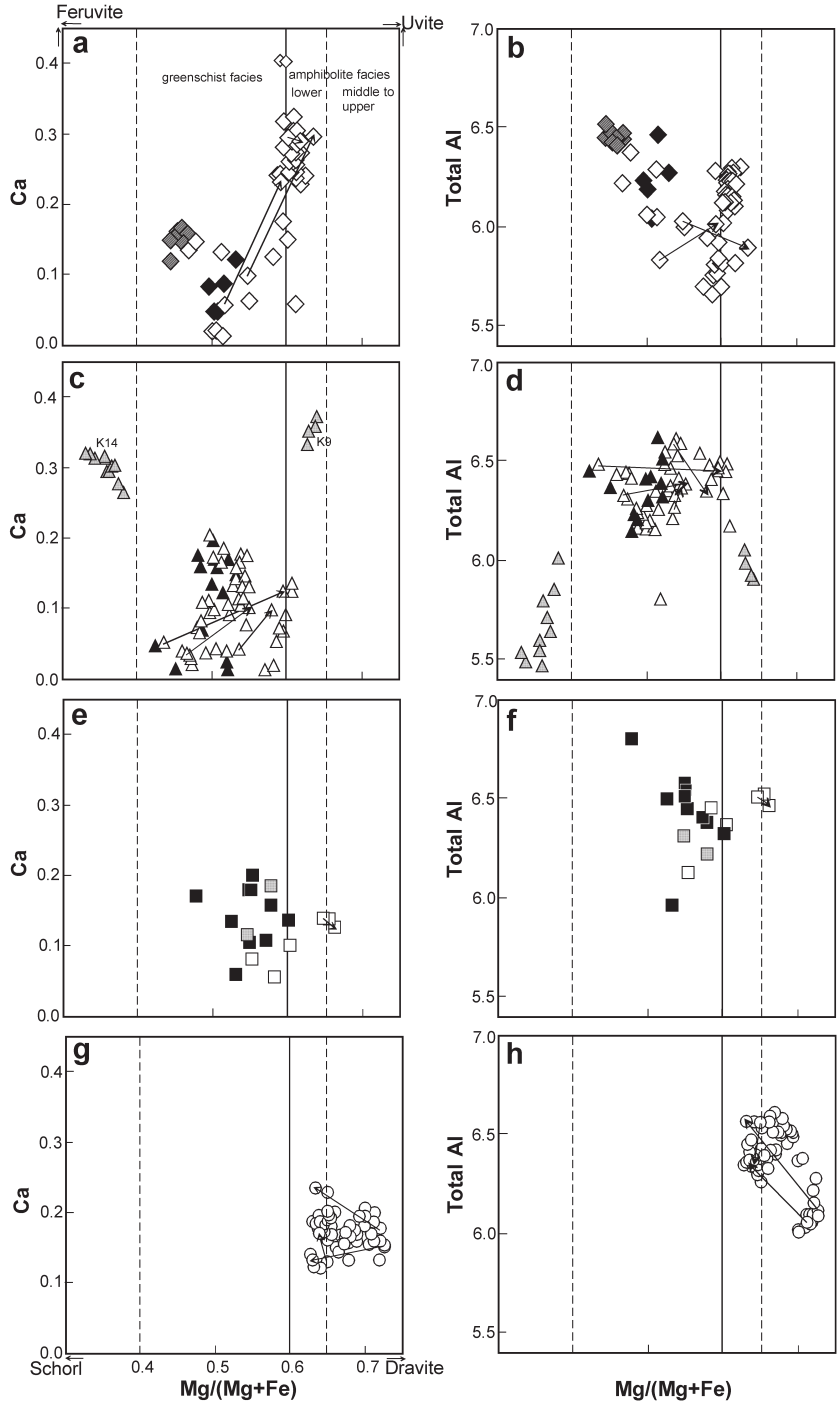

FIG. 6. Ca *vs.* Mg/(Mg+Fe^{tot}) and Al^{tot} *vs.* Mg/(Mg+Fe^{tot}) plots for the different tourmaline generations from the Sinai metasediments. The arrows indicate core → rim compositions of some tourmaline grains. (*a,b*) Melhaq tourmaline; (*c,d*) Wadi Kid−Umm Zariq tourmaline; (*e,f*) Taba tourmaline; and (*g,h*) G. Samra tourmaline. Symbols as in Fig. 3.

simultaneous decrease in Ca from the antilogous pole *c*(+) to the analogous pole *c*(−), whereas all other cations are virtually constant across the whole crystal (Fig. 7*a*).

The second type shows discontinuous zoning profiles often marked by steep concentration gradients with unsystematic differences in core−rim compositions (Fig. 7*b*,*c*,*d*). A tourmaline grain from a metasedimentary schist (sample K14) of the Wadi Kid−Wadi Umm Zariq area displays discontinuous optical zoning with an irregular, dark bluish-green core and a light green rim, formed during metamorphic growth. The detrital core is asymmetrically zoned in itself, a feature presumably inherited from its source-rock environment. Fe and Ca generally increase, whereas Al and the *X* site vacancies, □, decrease from the analogous *c*(−) towards the antilogous *c*(+) pole (cf. Dietrich, 1985; Sperlich *et al.*, 1996), with some slight recurrences (Fig. 7*b*). By contrast, there are abrupt changes and a nearly symmetrical element distribution at the border between the detrital core and the subhedral rim. Al, Ti, X_{Mg} and □ increase and Fe and Ca decrease drastically during the overgrowth stage, although with more or less distinct reversals towards the outermost rim (Fig. 7*b*). The other cations are virtually constant across the core, and only minor changes were measured for Si, Mg and Na in the outer rim. These chemical discontinuities suggest that only minor volume diffusion took place under the conditions of metamorphism (Henry and Dutrow, 1992), or may indicate that tourmaline grew at various stages, probably as a result of episodic boron availability (Gieré, 2001).

The euhedral tourmaline-3 crystal in the metapelite sample K9 from the Wadi Kid−Wadi Umm Zariq area is rather symmetrically zoned. It contains an irregular, orange-brown core of detrital origin (Fig. 2*e*), which is characterized by high Mg, Ca and Ti, but low Al, Fe and □ contents. Towards the surrounding, greenish neoblast, Mg, Ca, X_{Mg} and Ti decrease abruptly, while Al, Fe and □ increase gradually (Fig. 7*c*). Towards the thin, outermost rim, which shows a yellowish tint, there is a slight increase in the X_{Mg} ratio and the Al/Si ratio gains a maximum.

A tourmaline-3 crystal from the Samra metapsammopelites (sample Z3) contains no detrital core, but exhibits discontinuous chemical zoning with distinct compositional discontinuities (Fig. 7*d*), testifying to three successive growth stages I, II and III. Compared to the core formed during stage I, which has no systematic trend for

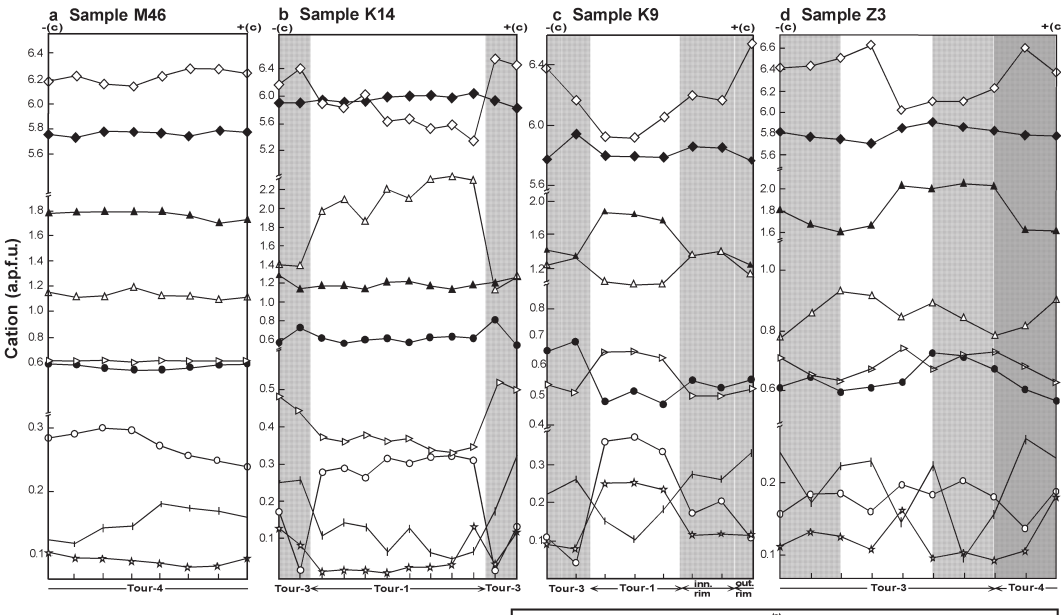

FIG. 7. Detailed compositional zoning of representative tourmaline crystals from: (*a*) Melhaq; (*b*,*c*) Kid, and (*d*) G. Samra metasediments (see text).

cationic variation; stage II is markedly poorer in Fe and Ti with nearly symmetrical distributions and decreasing X_{Mg} towards the rims. Ca is slightly enriched and Ti is depleted, while Mg and Na increase and Al decreases towards the antilogous *c*(+) pole only, indicating a distinct polarity. Due to its greater growth rate, the outer zone formed at stage III is restricted to the antilogous *c*(+) pole (Fig. 7*d*) and is characterized by enrichment of Al, Fe, Ti and □ and depletion of Mg, Na and X_{Mg} towards the rim.

Discussion

Tourmaline composition and host lithology

The composition of tourmaline can provide valuable information about the host lithology (Henry and Guidotti, 1985; Henry and Dutrow, 1992). Fe-rich tourmaline has long been regarded as a typical mineral for granitic and pegmatitic rocks (Selway *et al.*, 1999; Dyar *et al.*, 1999; Morgan VI and London, 1999; Novák *et al.*, 1999; Dutrow and Henry, 2000), while Mg-rich varieties are restricted to tourmalines formed by metasomatism or in sulphide deposits (Harraz and El-Sharkawi, 2001; Yu and Jiang, 2003). Metamorphic tourmaline has intermediate Mg/Fe ratios (Henry and Dutrow, 1992; Michailidis *et al.*, 1996; Sperlich *et al.*, 1996; Pesquera and Velasco, 1997; Dutrow *et al.*, 1999; Kawakami, 2001; Henry *et al.*, 2002; Kawakami and Ikeda, 2003). Indeed, the X_{Mg} values of the tourmaline crystals investigated fall in a wide range between 0.42 and 0.73 with Ca values of 0.02 to 0.40 a.p.f.u. thus pointing again to a metamorphic origin. In the Al-Fe^{tot}-Mg discrimination diagram (Fig. 5) of Henry and Guidotti (1985), the majority of the tourmaline grains analysed plots in the field of metapelites and metapsammites, either coexisting with an Al-saturating phase or not. Part of the Melhaq tourmaline, coexisting with epidote has high Ca and low Al values (Fig. 6*a*,*b*), typical for meta-calcpelitic host rocks (Fig. 5).

Dark orange-brown, detrital cores in tourmalines in sample K9 and T3, from the Umm Zariq and Taba metapelites, respectively, also plot in the fields of metapelitic and metapsammitic tourmalines (Fig. 5*b*,*c*). By contrast, bluish-green, detrital cores in tourmaline of sample K14 from the Umm Zariq metapelites form a distinct group with considerably lower X_{Mg} values (Fig. 4*c*,*d*). These grains could be derived from tourmaline-quartz rocks, formed by deuteric/hydrothermal alteration of granite, in the source area of the detritus (Fig. 5*b*). Our results clearly indicate that the detrital tourmaline grains, transported into the sedimentary basin, are derived from different rock types constituting the adjacent pre-Pan-African crystalline basement (cf. Krynine 1946; Henry and Dutrow, 1992).

In order to explore possible chemical relationships between near-peak tourmaline-3 and its host rock, correlation coefficients were calculated for some elements and parameters, using the bulk-rock analyses of Abu El-Enen *et al.* (2003, 2004, and unpubl.; see Table 4). Weak positive correlations were obtained for TiO_2 (0.47), CaO (0.49) and X_{Mg} (0.64), whereas FeO^{tot}, MgO and Na_2O showed virtually no correlation (0.09 to −0.23). This result indicates that the bulk rock chemistry of the individual samples has, at least, a small influence on the tourmaline composition, whereas metamorphic *P-T* conditions should have played a more important role (see below).

Neocrystallization of tourmaline in metamorphic rocks requires a source of boron. This could be supplied either from outside, i.e. by metasomatism, or inherited in the sedimentary precursors itself, i.e. in a closed system. Pelitic and psammitic sediments usually contain sufficient B to form tourmaline neoblasts during prograde metamorphism. Clay minerals, especially illite, and organic matter are extremely effective B adsorbers and are thus the most important sources for boron. Moreover, clay minerals and white mica may contain B in their tetrahedral sheets (e.g. Moran *et al.*, 1992; Grew, 1996; Henry and Dutrow, 1996, and references therein). Large amounts of mica in the tourmaline-bearing metasediments of the Sinai basement confirm that clay minerals, particularly illite, were an important constituent in the sedimentary precursors. Moreover, the occurrence of graphite in the Wadi Kid metapelites (Abu El-Enen *et al.*, 2003) indicates the presence of organic matter in some of the sedimentary protoliths. Prograde reactions, involving dehydration of illite and detrital white mica, transition from the 1*M* to the 2*M* polytype of illite, and conversion of organic matter into graphite can release boron to form significant amounts of tourmaline, up to temperatures corresponding to the lower-amphibolite facies (Weaver and Broekstra, 1984; Henry and Dutrow, 1990, 1996; Sperlich *et al.*, 1996). Towards higher metamorphic grade, breakdown of white mica by various dehydration reactions could also release boron.

TABLE 4. Bulk-rock composition (wt.%) of Sinai metasediments investigated.

Area	Melhaq					W. Kid–W. Umm Zariq						Taba	
Refer.	Abu El-Enen (unpublished data)					Abu El-Enen *et al.* (2003)						Abu El-Enen *et al.* (2004)	
	M28	M34	M38	M47	M50	K6	K9	K14	K22	K25	K35	T2	T12
SiO_2	69.53	73.25	71.87	50.48	50.48	60.22	59.21	56.55	63.52	62.08	63.67	55.77	63.98
TiO_2	0.25	0.25	0.47	0.89	0.91	0.96	0.93	0.91	0.93	1.07	0.75	1.09	0.76
Al_2O_3	14.66	12.58	14.01	17.28	15.85	19.11	21.26	22.22	19.15	22.19	19.89	21.12	15.97
Fe_2O_3	4.71*	3.34*	5.59*	17.18*	17.96*	1.45	0.96	1.97	0.96	1.55	1.18	3.52	0.91
FeO						5.00	4.68	4.64	4.55	4.09	3.52	5.18	4.55
MnO	0.09	0.08	0.08	0.51	0.44	0.10	0.10	0.18	0.11	0.12	0.06	0.09	0.10
MgO	1.25	1.64	0.58	4.27	4.41	2.42	1.59	1.61	1.66	1.27	1.38	3.20	2.56
CaO	1.90	2.81	0.17	0.74	0.62	1.38	1.48	1.76	1.14	0.96	0.67	1.83	2.31
Na_2O	1.51	0.78	0.28	1.66	1.09	2.50	2.47	2.02	1.94	1.25	1.09	2.56	3.72
K_2O	4.34	3.62	4.38	5.42	5.05	3.33	4.45	5.08	3.75	3.16	4.88	2.99	2.48
P_2O_5	0.14	0.03	0.08	0.13	0.12	0.09	0.07	0.04	0.02	0.05	0.04	0.16	0.22
LOI	1.40	1.31	1.99	1.78	2.51	3.13	2.06	2.56	1.82	1.70	2.33	1.78	1.55
Total	99.78	99.69	99.50	100.34	99.89	99.69	99.26	99.54	99.55	99.49	99.46	99.29	99.11
X_{Mg}	0.25	0.35	0.10	0.22	0.21	0.28	0.22	0.20	0.23	0.19	0.23	0.28	0.32

*: Total Fe as Fe_2O_3, X_{Mg}: $MgO/(MgO+FeO^{tot})$
LOI: loss on ignition

Development of tourmaline during metamorphism

From their textural position, the growth of tourmaline neoblasts can be inferred to correlate with specific stages of the *P-T* path, followed by the Sinai metasediments during Pan-African metamorphism. Tourmaline-2 included in various porphyroblasts, coexisting with quartz, muscovite, biotite, chlorite and ilmenite, should have grown on the prograde *P-T* path segment, starting at greenschist-facies conditions (Abu El-Enen *et al.*, 2003, 2004). Crystallization of tourmaline-3, orientated subparallel to, or wrapped by, the main schistosity, S_2, and grown in assemblage with garnet, staurolite, cordierite, andalusite and/or sillimanite has grown pre- to syn-D2, presumably under gradually increasing *P-T* conditions up to the metamorphic peak. These ranged from upper-greenschist facies in the southern Melhaq area *via* lower-amphibolite facies in the Kid area and pass to the upper-amphibolite facies in the Gabal Samra area. Moreover, chemical zonation of tourmaline-3 may reflect increasing *P-T* conditions from core to rim. Tourmaline-4 crystals crosscutting the S_2 foliation has crystallized post-D_2, probably just after the metamorphic peak or at the retrograde *P-T* path segment.

These assumptions, derived from textural evidence, are confirmed by the chemical composition of the different tourmaline generations. As was shown, e.g. by Henry and Dutrow (1996) and Sperlich *et al.* (1996), metamorphic tourmaline does not readily readjust its composition by volume diffusion, even at relatively high temperatures. Therefore, its chemistry can be used as a monitor for changing *P-T* conditions. In fact, tourmaline from the Sinai metasediments, supposedly grown at the prograde, peak and retrograde stage of the metamorphic evolution, respectively, displays differences in chemical compositions, especially in X_{Mg}. This can be demonstrated by looking at (1) individual, zoned tourmaline grains, (2) tourmaline grains of different textural position and (3) peak tourmaline from different areas.

(1) In zoned tourmaline of the metapelite sample K14 from the Wadi Kid-Wadi Umm Zariq area, the lowest X_{Mg} values of 0.33–0.38 are restricted to relict cores of detrital grains (Fig. 4*c*,*d*). The prograde evolution from the detrital core towards the rim is documented by an abrupt decrease in Fe at rather constant Mg, leading to a distinctly higher X_{Mg} value of 0.45–0.52, thus supporting its generation on the prograde *P-T* path up to near-peak metamorphic conditions (Fig. 7*b*). This increase could be related to the breakdown of chlorite (X_{Mg} 0.33–0.39) to form almandine-rich garnet (X_{Mg}

0.06−0.07) at the transition from the greenschist to the amphibolite facies.

The detrital core in tourmaline-3 of sample K9 has a distinctly larger X_{Mg} value of 0.63 than the surrounding neoblast, thus indicating derivation from relatively high-grade metamorphosed sediments in the source area. Within the neoblast itself, a small, renewed increase in X_{Mg} is recorded from core (0.50) to rim (0.52) which may reflect a slight increase in temperature. Moreover, the strong increase of Al towards the outermost rim may be explained by breakdown of white mica at the prograde *P-T* path.

For a different type of zonation, sample Z3, which has three successive growth stages (I, II and III), demonstrates no specific cationic variation for stage I, and increase in [only towards the antilogous (+) pole!] X_{Mg} and decrease in Fe from core to rim for stage II, while the distribution of Mg with its strong increase towards the antilogous pole + (*c*) only indicates a distinct polarity. The thin outer rim (stage III) at the antilogous pole *c*(+), is characterized by a decrease in Mg and X_{Mg}, and an increase in Fe (Fig. 7*d*). These features are related to crystallization of stages I and II near the metamorphic peak, while stage III was crystallized at the retrograde *P-T* branch. This is supported by retrograde replacement of garnet by chlorite and biotite observed in this sample.

(2) The best examples for compositional differences of tourmalines in different textural positions are provided by the metasediments of the Melhaq Formation. Prograde tormaline-2 and retrograde tourmaline-4 have X_{Mg} values of 0.49−0.53 and 0.43−0.47, respectively, whereas the great majority of near-peak tourmaline has X_{Mg} values of >0.56. Distinct differences between prograde (X_{Mg} 0.53−0.55) and peak tourmaline (X_{Mg} 0.65−0.67) were also recorded in the metasediments from the Taba metamorphic complex (Fig. 6*e*,*f*). In the Wadi Kid−Wadi Umm Zariq metapelites, prograde tourmaline−2 has X_{Mg} values of 0.42−0.52, whereas near-peak tourmaline-3 covers a much wider range between 0.44 and 0.61 (Fig. 6*c*,*d*), overlapping with that of tourmaline-2. This may be partly explained by an influence of the bulk-rock composition. However, looking at tourmaline grains within the same samples, the differences become obvious, e.g. in the samples K35, prograde tourmaline-2 has an X_{Mg} value of 0.49, while near-peak tourmaline-3 has an X_{Mg} value of 0.55. For sample K22, the respective X_{Mg} values are 0.53 and 0.59 (Table 2). We assume that the wide range of X_{Mg} values of near-peak tourmaline-3 reflects the transition from greenschist- to amphibolite-facies conditions during their growth (Fig. 6), which took place on the prograde *P-T* path and extended up to the metamorphic peak.

(3) The compositional variability of peak tourmaline-3 from metasediments in different metamorphic complexes of the Sinai basement, or in different areas of the same metamorphic complex, may partly reflect regional variations in *P-T* conditions attained at the culmination of the Pan-African metamorphic event. For instance, the highest X_{Mg} values of 0.65−0.66 and 0.64−0.73 (Table 2) were recorded for tourmaline-3 from the metasediments of the Taba and Feiran-Solaf complexes, respectively, which show peak-metamorphic assemblages corresponding to the middle- and upper-amphibolite facies. Moreover, the increase in metamorphic grade from the southern to the northern part of the Melhaq Formation, already recognized by Shimron (1984) and Furnes *et al.* (1985), is matched by an increase in the X_{Mg} values of matrix tourmaline-3, i.e. X_{Mg} varies from 0.50 in the southern to 0.62 in the northern part of the formation. On the other hand, matrix tourmaline-3 in metapelites of the rather small Wadi Kid−Wadi Umm Zariq area exhibits a relatively wide range of X_{Mg} (0.44−0.61), which points to crystallization of individual tourmaline grains at *P-T* conditions varying along the prograde *P-T* path up to the metamorphic peak. Comparing tourmaline from the Wadi Kid−Wadi Um Zariq and the Gebel Samra meta-sediments, a slight tendency for increasing Ca values with metamorphic grade is observed. On the other hand, the high Ca values in tourmalines coexisting with epidote from meta-calcpelites in the northern part of the Melhaq Formation are obviously controlled by the bulk-rock composition.

X_{Mg} of tourmaline could be used to draw tentative limits between tourmalines formed under different metamorphic conditions, possible exceptions being samples with extremely high or low X_{Mg} values in their bulk-rock composition. All the prograde tourmalines-2 investigated, which were formed with mineral assemblages typical of the greenschist facies have X_{Mg} <0.60. Therefore, this value might be used to designate the limit between the greenschist and the lower-amphibolite facies. This is confirmed by X_{Mg} values of 0.50−0.55, which were recorded for tourmalines of sample M28 from the Melhaq

Formation, containing a mineral assemblage of the upper-greenschist facies (Table 1). Moreover, cores and rims of zoned tourmalines from the Melhaq and the Wadi Kid−Wadi Umm Zariq areas show X_{Mg} values just below and above the proposed limit of 0.60, respectively (Fig. 6), which again relates to their crystallization at the *P-T* path segment extending from the prograde greenschist-facies to lower amphibolite-facies conditions at the metamorphic peak. Similar low to moderate X_{Mg} values of 0.21−0.42 were reported for tourmaline from low-grade metasediments of the Stavelot Massif, Belgium (Van den Bleeken *et al.*, 2007). The border between the lower- and middle to upper-amphibolite facies, respectively, might be tentatively set at $X_{Mg} \approx 0.65$ (Fig. 6). Similar X_{Mg} values of 0.65−0.77 are given by Kawakami (2001) for rim compositions of tourmalines from migmatites formed under upper amphibolite-facies conditions at the Ryoke metamorphic belt, Japan. These limits conform to the results of petrological analyses in various parts of the Sinai basement (Shimron, 1984; Furnes *et al.*, 1985; Abu El-Enen *et al.* 2003, 2004, unpubl.).

Application of the tourmaline-biotite geothermometer

Assuming that intercrystalline partitioning of Fe and Mg between tourmaline and biotite is a function of temperature, Colopietro and Friberg (1987) proposed a tourmaline-biotite geothermometer, which was empirically calibrated by applying garnet-biotite geothermometry to metapelites of the garnet, biotite and sillimanite zones. They arrived at the equation: $\ln K_D = -3150/T\,(K) + 4.52$, where $K_D = (Mg/Fe)_{tur}/(Mg/Fe)_{bt}$, defining a positive slope of their regression line in the K_D *vs.* *T* diagram. A positive correlation between K_D and *T* was also recorded by Henry and Dutrow (1994), at least up to temperatures of 600ºC. However, using a somewhat different approach, these authors obtained a shallower slope of the regression line and showed that, above 600ºC, K_D decreases with temperature. They pointed out that crystal-chemical complexities of the tourmaline structure reduce the efficiency of the Mg-Fe partitioning between tourmaline and biotite as a useful geothermometer. In the contact aureole of the Miocene Tinos granite (Cyclades islands, Greece), part of the tourmaline-biotite temperatures broadly conform to the mineral isograds mapped, whereas temperatures far too low were recorded in certain areas (Bröcker and Franz, 2000). These authors explain this fact "by retrograde cation exchange in biotite and refractory behaviour of tourmaline" or, alternatively, by "systematic shortcomings of this method".

Despite these reservations, we applied the tourmaline-biotite geothermometer of Colopietro and Friberg (1987) to prograde, peak and retrograde tourmalines from the metasediment samples investigated and obtained reasonable results. The temperatures calculated compare well with those from our previous estimates (Abu El-Enen *et al.*, 2003, 2004; Abu El-Enen and Makroum, 2003; Abu El-Enen, unpubl.), and there is a strong positive correlation ($r = 0.91$) with results from the garnet-biotite geothermometer (in the formulation of Kleemann and Reinhardt, 1994) in the same sample (Table 5).

In the Melhaq Formation, there is a general increase in peak tourmaline-biotite temperatures from ~485ºC in the southern part up to 570ºC in the central area. For sample M38 from the central area, nearly identical peak temperatures of 568ºC and 554ºC were obtained using the tourmaline-biotite and garnet-biotite geothermometer, respectively. In the northern area, tourmaline-biotite temperatures for both prograde tourmaline-2 (563ºC) and retrograde tourmaline-4 (507ºC and 551ºC) in sample M47 and M50 are distinctly lower than the peak garnet-biotite temperature of 645ºC in sample M50, which in turn is distinctly higher than the peak tourmaline-biotite and garnet-biotite temperatures in the central Melhaq area (Table 5).

In the Wadi Kid−Wadi Um Zariq metapelites, peak temperatures calculated by the tourmaline-biotite geothermometer are between 556 and 572ºC, conforming well to respective garnet-biotite temperatures of 565−575ºC, as well as to garnet-staurolite (Hodges and Spear, 1982) and garnet-cordierite temperatures (Bhattacharya *et al.*, 1988) of 580 and 585ºC, respectively, at pressures of 3−5 kbar. Application of the internally consistent thermodynamic data set of Holland and Powell (1998) yielded 591±28ºC and 4.2±0.9 kbar (Abu El-Enen *et al.*, 2003). Tourmaline-biotite temperatures for prograde tourmaline-2 of 506−540ºC are consistently lower than the respective peak temperatures (Table 5).

In the Taba complex, only one tourmaline-biotite temperature of 564ºC was obtained for peak tourmaline, which conforms to garnet-biotite and garnet-staurolite temperatures of 550−590ºC and 580ºC, respectively, at pressures of 3−5 kbar;

TABLE 5. Temperature estimates of the investigated samples using tourmaline-biotite geothermometry, compared with the results from the garnet-biotite geothermometer of Kleemann and Rheinhardt (1994), given by Abu El-Enen *et al.* (2003, 2004). Relevant pressures (kbar), for which garnet-biotite temperatures were calculated, are given in parentheses.

Area	Sample no.	Tur-Bt geothermometry (ºC)			Grt-Bt geothermometry (ºC)	
		prograde	peak	retrograde	prograde	peak
Melhaq						
Southern	M28		509±21			
	M34		485±20			
Central	M38		568±17			554±8 (3.8)
	M43		533±11			
	M46		524±4			
Northern	M47			551±6		
	M50	563±12		507±6		645±16 (4.8)
W. Kid–W. Umm Zariq						
	K6		572±9			560±5 (3.5)
	K9	540±1	571±12			565±13 (2.4)
	K14		563±7			565 (3.5)
	K22	527	570±11			575±5 (4.1)
	K25	506±6	571±5			570±6 (4.1)
	K35	515±2	556±4			565±12 (4.0)
Taba belt						
	T2	450±6			515±3(2.7)	568±4 (3.4)
	T10	462±12			540±4(3.3)	557±7 (2.9)
	T12		564±7			585±7 (4.2)
G. Sammra						
	Z1	573±14	632±12			627±23 (4.5)

a *P-T* pseudosection led to a similar result (Abu El-Enen *et al.*, 2004). For prograde tourmaline, distinctly lower temperatures of 450−462ºC were calculated by tourmaline-biotite thermometry, whereas garnet-biotite temperatures related to the prograde *P-T* path vary between 480 and 540ºC. Conventional geothermobarometry of meta-psammopelites from the Feiran-Solaf complex yielded peak temperatures between 600 and 670ºC and pressures of ~4.5 kbar (Abu El-Enen, unpubl.) using Kleemann and Reinhardt (1994) and Hoisch (1990), respectively. Temperatures of 632ºC for a peak tourmaline-biotite pair and of 627ºC for a garnet-biotite pair in the same sample are well within this range, whereas a prograde tourmaline-biotite pair gave a distinctly lower 573ºC. These consistent results seem to indicate that the tourmaline-biotite thermometer of Colopietro and Friberg (1987) is a useful approach even at temperatures above 600ºC.

Conclusions

Based on detailed petrographic and microprobe analyses of tourmaline in metasediments from different areas in the Pan-African basement of the Sinai Peninsula, the following conclusions can be drawn:

(1) Tourmaline from the metasedimentary rocks of the Sinai exhibit textural and chemical features that relate to the evolution of regional metamorphism and deformation of the host rocks. Prograde inclusions of tourmaline-2 in various porphyroblasts testify to the prograde *P-T* path; tourmaline-3 oriented subparallel to, and wrapped by, the main foliation, S_2, crystallized along the prograde path up to the metamorphic culmination, and tourmaline-4 crosscutting the S_2 schistosity, was formed post-peak, on the retrograde *P-T* path. Cores in prograde and peak tourmaline neoblasts are interpreted as detrital grains (tourmaline-1), testifying to the source area(s) of the sedimentary precursors.

(2) With increasing *P-T* conditions at the metamorphic culmination, near-peak tourmalines-3 and -4 increase in size, but decrease in abundance.

(3) The tourmaline crystals investigated belong exclusively to the alkaline tourmaline group; they have schorl–dravite composition with minor uvite-feruvite and foitite/Mg-foitite components.

(4) In general, the chemical composition is typical for tourmalines in metapelites and metapsammites, coexisting or not coexisting with an Al-saturating phase. Meta-calcpelites from the Melhaq Formation contain dravites, which are somewhat richer in Ca and poorer in Al. Detrital cores in tourmaline neoblasts (tourmaline-1) have variable composition testifying to different rocks and/or source regions in the adjacent pre-Pan-African basement. Detrital cores in sample K14 with distinctly lower X_{Mg} values and relatively poor in Al may have been derived from Fe^{3+}-rich quartz-tourmaline rocks (hydrothermally altered granites), while detrital cores of samples K9 and T3 with moderately to distinctly higher X_{Mg} may have been derived from pre-existing metapelitic-metapsammitic rocks.

(5) The tourmaline neoblasts surrounding these cores have grown during prograde metamorphism under increasing, greenschist to amphibolite-facies, *P-T* conditions. This crystallization took place in a virtually closed system. In addition to detrital tourmaline grains, boron was provided by the breakdown of clay minerals and organic matter, which are effective B adsorbers, and of white micas, which may have contained B in their tetrahedral layers.

(6) The chemical compositions of tourmaline, especially X_{Mg} = Mg/(Mg+Fe^{tot}) values of the tourmaline investigated, are a good monitor for *P-T* conditions, attained by the host metapelites and metapsammites. Except for extremely high and low X_{Mg} values of the host rock, the limit between greenschist and amphibolite facies might be tentatively set at $X_{Mg}^{tur} \approx 0.60$, and between lower- and upper-amphibolite facies at $X_{Mg}^{tur} \approx 0.65$. The empirically calibrated tourmaline-biotite geothermometer of Colopietro and Friberg (1987) yielded reasonable results, conforming well to temperatures obtained by the garnet-biotite geothermometer of Kleemann and Reinhardt (1994) and other conventional geothermometers. In order to obtain reasonable temperature information by applying the tourmaline-biotite thermometer, the textural positions of tourmaline should be defined carefully, to distinguish between prograde, near-peak and retrograde generations of tourmaline.

Acknowledgements

The paper benefited considerably from constructive reviews by Thomas Will, Paul Hoskin and two anonymous reviewers, which are gratefully acknowledged. Thanks are due to Uli Schüssler for his advice and help with the EMP analyses. Financial support by the Deutsche Forschungsgemeinschaft (grant OK 2/62-1), Deutscher Akademischer Austauschdienst, Mineralogisches Institut, Universität Würzburg, and Department of Geology, University of El Mansoura, is appreciated.

References

Abd El-Shakour, Z.A. (2005) *Metamorphic evolution of migmatites from Sinai, Egypt*. Unpublished MSc thesis, University of El Mansoura, Egypt, 135 pp.

Abu El-Enen, M.M. (1995) *Geological, geochemical and mineralogical studies on the metamorphic rocks between Wadi Umm-Maghra and Wadi Tweiba, SE Sinai, Egypt*. Unpublished PhD thesis, University of El Mansoura, Egypt, 172 pp.

Abu El-Enen, M.M. and Makroum, F.M. (2003) Tectonometamorphic evolution of the northeastern Kid complex, SE Sinai, Egypt. *Annals of the Geological Survey of Egypt*, **26,** 19–37.

Abu El-Enen, M.M., Zalata, A.A., El-Metwally, A.A. and Okrusch, M. (1999) Orthogneisses from the Taba metamorphic complex, SE Sinai, Egypt: Witnesses for granitoid magmatism at an active continental margin. *Neues Jahrbuch für Mineralogie Abhandlungen*, **175**, 53–81.

Abu El-Enen, M.M., Okrusch, M. and Will, T.M. (2003) Metapelite assemblages in the Umm Zariq schists, central western Kid Complex, Sinai Peninsula, Egypt. *Neues Jahrbuch für Mineralogie Abhandlungen*, **178**, 277–306.

Abu El-Enen, M.M., Will, T.M. and Okrusch, M. (2004) P-T evolution of the Taba metamorphic complex, Egypt: Constraints from the metapelite assemblages. *Journal of African Earth Sciences*, **38**, 59–78.

Bhattacharya, A., Mazumdar, A.C. and Sen, S.K. (1988) Fe-Mg mixing in cordierite: Constraints from natural data and implications for cordierite-garnet thermometry in granulites. *American Mineralogist*, **73**, 338–344.

Bröcker, M. and Franz, L. (2000) The contact aureole on Tinos (Cyclades, Greece): tourmaline-biotite geothermometry and Rb-Sr geochronology.

Mineralogy and Petrology, **70**, 257–283.

Brooijmans, P., Blasband, B., White, S.H., Visser, W.J. and Dirks, P. (2003) Geothermobarometric evidence for a metamorphic core complex in Sinai, Egypt. *Precambrian Research*, **123**, 249–268.

Colopietro, M.R. and Friberg, L.M. (1987) Tourmaline-biotite as a potential geothermometer for metapelites; Black Hills, South Dakota. *Geological Society of America Abstracts with Programs*, **19**(7), p. 624.

Cosca, M.A., Shimron, A. and Caby, R. (1999) Late Precambrian metamorphism and cooling in the Arabian-Nubian Shield: Petrology and $^{40}Ar/^{39}Ar$ geochronology of metamorphic rocks of the Elat area (southern Israel). *Precambrian Research*, **98**, 107–127.

Dietrich, R.V. (1985) *The Tourmaline Group*. Van Nostrand Reinhold Co., New York, 300 pp.

Dixon, T.H. and Golombek, M.P. (1988) Late Precambrian crustal accretion rates in northeast Africa and Arabia. *Geology*, **16**, 991–994.

Dutrow, B.L. and Henry, D.J. (2000) Complexly zoned fibrous tourmaline, Cruzeiro mine, Minas Gerais, Brazil: A record of evolving magmatic and hydrothermal fluid. *The Canadian Mineralogist*, **38**, 131–143.

Dutrow, B.L., Foster Jr, C.T. and Henry, D.J. (1999) Tourmaline-rich pseudomorphs in sillimanite zone metapelites: Demarcation of an infiltration front. *American Mineralogist*, **84**, 794–805.

Dyar, M.D., Guidotti, C.V., Core, D.P., Wearn, K.M., Wise, M.A., Francis, C.A., Johnson, K., Brady, J.B., Robertson, J.D. and Cross, L.R. (1999) Stable isotopes and crystal chemistry of tourmaline across pegmatite – country rock boundaries at Black Mountain and Mount Mica, southwestern Maine, U.S.A. *European Journal of Mineralogy*, **11**, 281–292.

El-Gaby, S. and Ahmed, A.A. (1980) The Feiran-Solaf gneiss complex, SW of Sinai. Pp. 95–105 in: *Evolution and Mineralization of the Arabian-Nubian Shield* (P.G. Coory and S.A. Tahoun, editors). Institute of Applied Geology (Jeddah, Saudi Arabia), **4**.

El-Shafei, M.K. and Kusky, T.M. (2003) Structural and tectonic evolution of the Neoproterozoic Feiran-Solaf metamorphic complex, Sinai Peninsula: Implication for the closure of Mozambique Ocean. *Precambrian Research*, **123**, 269–293.

El-Tokhi, M. (1990) *Petrological, geochemical and experimental studies on migmatite rocks of Feiran area, S. Sinai, Egypt*. Unpublished PhD thesis, Karlsruhe, Germany, 98 pp.

Eyal, Y. (1980) The geological history of the Precambrian rocks between Wadi Tweiba and Wadi Um-Mara, NE Sinai. *Israel Journal of Earth Science*, **29**, 53–66.

Furnes, H., Shimron, A.E. and Roberts, D. (1985) Geochemistry of volcanic arc sequences in the southeastern Sinai Peninsula and plate tectonic implication. *Precambrian Research*, **29**, 359–382.

Gieré, R. (2001) Geochemical and tectonic significance of tourmaline rich metasedimentary rocks in the central Alps. *Geological Society of America, Abstracts with Program*, **33**.

Grew, E.S. (1996) Borosilicates (exclusive tourmaline) and boron in rock-forming minerals in metamorphic environments. Pp. 387–502 in: *Boron: Mineralogy, Petrology, and Geochemistry* (E.S. Grew and L.M. Anovitz, editors). *Reviews in Mineralogy*, **33**, Mineralogical Society of America, Washington, D.C.

Grice, J.D. and Ercit, T.S. (1993) Ordering of Fe and Mg in tourmaline crystal structure: The correct formula. *Neues Jahrbuch für Mineralogie Abhandlungen*, **165**, 245–366.

Harraz, H.Z. and El-Sharkawy, M.F. (2001) Origin of tourmaline in metamorphosed Sikait pelitic complex, south Eastern Desert, Egypt. *Journal of African Earth Sciences*, **33**, 391–416.

Hashad, M.H. (2001) Chemical characteristics and genesis of Wadi Sikait tourmaline. *Egyptian Mineralogist*, **13**, 1–26.

Hawthorne, F.C. and Henry, D.J. (1999) Classification of the minerals of the tourmaline group. *European Journal of Mineralogy*, **11**, 201–215.

Henry, D.J. (2003) Tourmaline as a geochemical tape recorder in metamorphic rocks. *Geological Society of America, Abstracts with Program*, **35**(6), p. 397.

Henry, D.J. and Guidotti, C.V. (1985) Tourmaline as a petrogenetic indicator mineral: an example from the staurolite-grade metapelites of NW Maine. *American Mineralogist*, **70**, 1–15.

Henry, D.J. and Dutrow, B.L. (1990) Ca-substitution in Li-poor aluminous tourmaline. *The Canadian Mineralogist*, **28**, 111–124.

Henry, D.J. and Dutrow, B.L. (1992) Tourmaline in a low grade clastic metasedimentary rock: an example of the petrogenetic potential of tourmaline. *Contributions to Mineralogy and Petrology*, **112**, 203–218.

Henry, D.J. and Dutrow, B.L. (1996) Metamorphic tourmaline and its petrologic application. Pp. 503–557 in *Boron: Mineralogy, Petrology, and Geochemistry* (E.S. Grew and L.M. Anovitz, editors). Reviews in Mineralogy, **33**, Mineralogical Society of America, Washington, D.C.

Henry, D.J., Dutrow, B.L. and Selverstone, J. (2002) Compositional polarity in replacement tourmaline – an example from the Tauern Window, Eastern Alps. *Geological Materials Research*, **4**, 23 pp.

Hodges, K.V. and Spear, F.S. (1982) Geothermometry, geobarometry and the Al_2SiO_5 triple point at Mt. Moosilake, New Hampshire. *American Mineralogist*,

67, 1118–1134.

Hoisch, D.T. (1990) Experimental calibrations of six geobarometers for the mineral assemblage quartz + muscovite + biotite + plagioclase + garnet. *Contributions to Mineralogy and Petrology*, **104**, 225–234.

Holland, T.J.B. and Powell, R. (1998) An internally consistent thermodynamic data set for phases of petrological interest. *Journal of Metamorphic Geology*, **16**, 309–343.

Kawakami, I. (2001) Tourmaline breakdown in the migmatite zone of the Ryoke metamorphic complex, SW Japan. *Journal of Metamorphic Geology*, **19**, 61–75.

Kawakami, T. and Ikeda, T. (2003) Boron in metapelites controlled by the breakdown of tourmaline and retrograde formation of borosilicates in the Yanai area, Ryoke metamorphic complex, SW Japan. *Contributions to Mineralogy and Petrology*, **145**, 131–150.

Kleemann, U. and Reinhardt, J. (1994) Garnet-biotite thermometry revisited: The effect of Al^{VI} and Ti in biotite. *European Journal of Mineralogy*, **6**, 925–941.

Kretz, R. (1883) Symbols for rock forming minerals. *American Mineralogist*, **68**, 277–279.

Kröner, A., Greiling, R., Reischmann, T., Hussein, I.M., Stern, R.J., Dürr, S. and Zimmer, M. (1987) Pan African crustal evolution in the segment of northern Africa. Pp. 235–257 in: *Proterozoic Lithosphere Evolution* (A. Kröner, editor). International Lithosphere Program Publication, **130**. American Geophysical Union, Geodynamic Series **17**. Washington, D.C.,

Krynine, P.D. (1946) The tourmaline group in sediments. *Journal of Geology*, **54**, 65–87.

Michailidis, K., Kassoli-Fournaraki, A. and Dietrich, R.V. (1996) Origin of zoned tourmalines in graphite-rich metasedimentary rocks from Macedonia, northern Greece. *European Journal of Mineralogy*, **8**, 393–404.

Moran, A.E., Sisson, V.B. and Leeman, W.P. (1992) Boron in subducted oceanic crust and sediments: Effects of metamorphism and implications for arc magma compositions. *Earth and Planetary Science Letters*, **111**, 331–349.

Morgan VI, G.B. and London, D. (1999) Crystallization of the Little Three layered pegmatite-aplite dike, Ramona District, California. *Contributions to Mineralogy and Petrology*, **136**, 310–330.

Navon, O. and Reymer, A.P.S. (1984) Stratigraphy, structures and metamorphism of Pan-African age in central Kid, southeastern Sinai. *Israel Journal of Earth Science*, **33**, 135–149.

Novák, M., Selway, J.B., Černý, P., Hawthorne, C. and Ottolini, L. (1999) Tourmaline of the elbaite-dravite series from an elbaite-subtype pegmatite at Bližna, southern Bohemia, Czech Republic. *European Journal of Mineralogy*, **11,** 557–568.

Pesquera, A. and Velasco, F. (1997) Mineralogy, geochemistry and geological significance of tourmaline-rich rocks from the Paleozoic Cino Villas massif (western Pyrenees, Spain). *Contributions to Mineralogy and Petrology*, **129**, 53–74.

Reymer, A.P.S., Matthews, A. and Navon, O. (1984) Pressure-temperature conditions in the Wadi Kid metamorphic complex: implications for the Pan-African event in SE Sinai. *Contributions to Mineralogy and Petrology*, **85**, 336–345.

Rogers, J.J.W., Unrug, R. and Sultan, M. (1995) Tectonic assembly of Gondwana. *Journal of Geodynamics*, **19**, 1–34.

Selway, J.B., Novák, M., Černý, P. and Hawthorne, F.C. (1999) Compositional evolution of tourmaline in lepidolite-subtype pegmatites. *European Journal of Mineralogy*, **11**, 569–584.

Shackleton, R.M. (1986) Precambrian collision tectonics in Africa. Pp. 329–349 in: *Collision Tectonics* (M.P. Coward and A.C. Reis, editors). Special Publication **19**, Geological Society, London.

Shackleton, R.M. (1996) The final collision zone between East and West Gondwana: where is it? *Journal of African Earth Sciences*, **23**, 271–287.

Shimron, A.E and Zwart, H.J (1970) The occurrence of low-pressure metamorphism in the Precambrian of the middle-east and northeast Africa. *Geologie en Mijnbouw*, **45**, 369–374.

Shimron, A.E. (1980) Proterozoic island arc volcanism and sedimentation in Sinai. *Precambrian Research*, **12**, 437–458.

Shimron, A.E. (1984) Evolution of the Kid Group, southeast Sinai Peninsula: thrusts, mélanges and implication for accretionary tectonics during the Late Proterozoic of the Arabian-Nubian Shield. *Geology*, **12**, 242–247.

Slack, J.F. and Coad, P.R. (1989) Multiple hydrothermal and metamorphic events in the Kidd Creek volcanogenic massive sulfide deposits, Timmins, Ontario: Evidence from tourmaline and chlorites. *Canadian Journal of Earth Sciences*, **26**, 694–715.

Sperlich, R. (1990) *Zoning and crystal chemistry of tourmalines in prograde metamorphic sequences of the Central Alps*. Unpublished PhD thesis, University of Basel, Switzerland (not seen).

Sperlich, R., Gieré, R. and Frey, M. (1996) Evolution of compositional polarity and zoning in tourmaline during prograde metamorphism of sedimentary rocks in the Swiss Central Alps. *American Mineralogist*, **81**, 1223–1236.

Stern, R.J. (1994) Arc assembly and continental collision in the Neoproterozoic East African Orogen: implications for consolidation of

Gondwanaland. *Annual Reviews in Earth and Planetary Sciences*, **23**, 319–351.

Stern, R.J. (2002) Crustal evolution in the East African Orogen: a neodymium isotopic perspective. *Journal of African Earth Sciences*, **34**, 109–117.

Teklay, M., Kröner, A., Mezger, K. and Oberhänsli, R. (1998) Geochemistry, Pb-Pb single zircon ages and Nd-Sr isotope composition of Precambrian rocks from southern and eastern Ethiopia: implications for crustal evolution in East Africa. *Journal of African Earth Sciences*, **26**, 207–227.

Van den Bleeken, G., Corteel, C. and Van den Haute, P. (2007) Epigenetic to low-grade tourmaline in the Gdoumont metaconglomerates (Belgium): A sensitive probe of its chemical environment of formation. *Lithos*, **95**, 165–176.

Weaver, C.E. and Broekstra, B.R. (1984) Illite-mica. Pp. 67–199 in: *Shale Slate Metamorphism in Southern Appalachians* (C.E. Weaver *et al.*, editors). Elsevier, Amsterdam.

Yu, J.M. and Jiang, S.Y. (2003) Chemical composition of tourmaline from the Yunlong tin deposits, Yunnan, China: Implication for ore genesis and mineral exploration. *Mineralogy and Petrology*, **77**, 67–84.

Zen, E.-An. (1981) Metamorphic mineral assemblages of slightly calcic pelitic rocks in and around the Taconic Allochthon, southwestern Massachusetts and adjacent Connecticut and New York. *US Geological, Survey*, Professional Paper, **1113**, 1–128.